FINAL SCIENTIFIC REPORT

Regarding the project implementation in the period 2020–2022

Project title: "**The behaviour of new multicomponent polymeric systems in simulated environmental conditions for flame retardant coating materials**" Code: **PN–III–P1–1.1–TE–2019–0604**

Proposed and achieved objectives

Stage 1: October–December 2020
Objectives and activities:
> **1. The obtaining of the semi–interpenetrating polymer networks (S–IPNs) based on crosslinked epoxy resin and oligophosphonate (OP) and the characterization of the materials**
> **1.1.** *Scientific documentation*
> **1.2.** *Investigation of modern instrumental techniques and methods*
> **1.3.** *Synthesis and structural characterization of the precursor to the OP. Synthesis and structural characterization of the OP.*
> The following activities were undertaken during this stage of the project:

- ✓ creation and analysis of a database with recent information in the field of phosphorus based monomers and polymers, as well as epoxy resins (books, reviews and scientific articles, patents);
- ✓ a selection of the methods of investigation and characterization, based on the analyzed literature data;
- ✓ purification of the monomers and solvents for the synthesis of the precursor to the OP;
- ✓ synthesis of the monomers by classic polycondensation and addition reactions.

Stage 2: January–December 2021
Objectives and activities:
> **2. The obtaining and characterization of the S–IPNs based on OP and epoxy resin (continuation from Stage 1). The thermal and fire behavior of the S–IPNs.**
> **2.1**. *The obtaining and characterization of the S–IPNs based on OP and epoxy resin*
> **2.2**. *The microbiological testing of the S–IPNs*
> **2.3**. *The thermal and fire behavior of the S–IPNs*
> The following activities were undertaken during this stage of the project:

- ✓ obtaining of the S–IPNs based on OP and epoxy resin
- ✓ structural characterization of the S–IPNs by FTIR and SEM-EDX investigation techniques;
- ✓ microbiological testing of the S–IPNs resistance to the fungal strains *Penicillium chrysogenum*, *Cladosporium cladosporioides* and *Aspergillus brasiliensis*;
- ✓ differential scanning calorimetry (DSC) and comparative thermal degradation studies in inert and thermo–oxidative atmospheres by thermogravimetric analysis (TGA);
- ✓ determination of non–isothermal kinetic parameters of thermal degradation;
- ✓ analyses of evolved gases during termal degradation by TGA–FTIR and Py–GC–MS coupled techniques;
- ✓ flame resistance study of the S–IPNs by microscale cone calorimetry (MCC) and UL–94 VB small scale fire test.

Stage 3: January–October 2022
Objectives and activities:
> **3. Accelerated UV aging correlated with flame resistance capacity of the S–IPNs**
> **3.1.** *Photochemical behavior study of the S–IPNs*
> **3.2.** *Promoting the project visibility*
> **3.3.** *Dissemination of the results obtained throughout the entire project implementation*
> The following activities were undertaken during this stage of the project:

- ✓ evaluation of the influence of wavelength and irradiation intensity;
- ✓ investigation of surface properties by SEM–EDX;
- ✓ determination of optical (color) and structural (UV-Vis) properties;
- ✓ correlation between photochemical behavior and flame resistance capacity of the S–IPNs;
- ✓ scientific coordination and presentation of the results on the project web page as well as the final dissemination.

Presentation of the obtained results, of the achieved result indicators; of the recorded non-achievements compared to the results estimated by the financing application (if applicable), with their justification

No.	Deliverables/planned indicators	No.	Deliverables/achieved indicators	No.
1.	OP synthesis	1	OP synthesis	1
2.	Obtaining of S-IPNs	3	Obtaining of S-IPNs	3
3.	ISI Scientific articles	2	ISI Scientific articles	7
4.	Conferences	4	Conferences	6
5.	Oral communications/posters presented at national and international conferences	4	Oral communications/posters presented at national and international conferences	13
6.	Technical and scientific report on the obtaining and characterization of the S-IPNs based on crosslinked epoxy resin and OP	1	Technical and scientific report on the obtaining and characterization of the S-IPNs based on crosslinked epoxy resin and OP	1
7.	Technical and scientific report on the obtaining and characterization of the S-IPNs (continuation from the report on Stage 1); thermal behavior, flame resistance studies, and accelerated UV aging correlated with the flame resistance capacity of the S-IPNs	1	Technical and scientific report on the obtaining and characterization of the S-IPNs (continuation from the report on Stage 1); thermal behavior, flame resistance studies, and accelerated UV aging correlated with the flame resistance capacity of the S-IPNs	1
8.	Webpage	1	Webpage	1
9.	Scientific and technical report at the end of each stage	3	Scientific and technical report at the end of each stage	3

All the objectives and activities proposed for these stages were fully achieved and are further presented in detail in the scientific and technical description.

Scientific and technical description of the activities for each stage

Stage 1. The obtaining of the semi–interpenetrating polymer networks (S–IPNs) based on crosslinked epoxy resin and oligophosphonate (OP) and the characterization of the materials

Activity 1.1. Scientific documentation: - Creation of a database with recent information in the field of phosphorus based monomers and polymers, as well as epoxy resins (books, reviews and scientific articles, patents); Analysis of informational data

The research team created a database with recent information in the field of polymer behavior under the action of environmental factors regarding flame retardant phosphorus based monomers, polymers and multicomponent polymer systems. Documentation was also made in the field of modern instrumental techniques and methods for defining the study problem and developing the experimental plan. In this sense, recent specialized literature (scientific articles, books, patents, doctoral theses) were procured and the methods for investigating the degradability of the obtained polymer systems were selected. The activity also aimed at documenting recent data in the specialized literature regarding the correlation of thermal, microbiological and accelerated UV aging mechanisms of polymers with their flame resistance for environmental exposure. The activity was fully achieved.

Activity 1.2. Investigation of modern instrumental techniques and methods; Selection of investigation and characterization methods based on literature information

Structural investigations of the materials were undertaken by: Fourier transform infrared spectroscopy (**FTIR**), nuclear magnetic resonance (**^{1}H-NMR**), scanning electron microscopy (**SEM**) and energy dispersive X–ray spectroscopy (**EDX**). Thermogravimetric analysis (**TGA**) in inert and oxidative atmospheres were used for the thermal degradation of the materials. The resulted gaseous products were identified with **TGA–FTIR** and **Py–GC–MS** coupled devices. The flame retardant capacity was tested by microscale cone calorimetry **(MCC)**. A medium pressure mercury lamp (100 W) at 365 nm was used for the photoirradiation of the multicomponent materials. Color modification studies during photoirradiation were made with a colorimeter. **UV–Vis** spectroscopy with an integrated sphere was used for reflectance measurements.

Activity 1.3. Synthesis and structural characterization of the precursor to the OP; Synthesis and structural characterization of the synthesized OP.

1.3.1. Synthesis and structural characterization of the precursor to the OP

4,4'-terephthalylidene–bis(p-hydroxyaniline) (compound 1), was synthesized by reacting 4–aminophenol (0.2 mol), terephthalaldehyde (0.1 mol) and a catalytic amount of 4-toluenesulfonic acid dissolved in 300 mL dry ethanol (Scheme 1). The mixture was refluxed for 3 h under stirring. After cooling at room temperature the product was separated by precipitation over a water-ice mixture, filtered, washed with distilled water and dried under vacuum. The final product was recrystallized from toluene.

The synthesis of bis((6-oxido-6H-dibenz[c,e][1,2]oxaphosphorinyl)-(4-hydroxyaniline)-methylene)-1,4-phenylene (*the precursor to the OP*), was achieved by reacting compound 1 with DOPO. Compound 1 (14.62 g, 0.0462 mol), DOPO (20 g, 0.0926 mol) and dried ethanol (103 mL) were introduced into a round flask equipped with a condenser and a magnetic stirrer. The mixture was stirred at 50 °C for 12 h under nitrogen atmosphere. The resulting precipitate was filtered, washed with ethanol and dried under vacuum (yield: 90%). **Characterization: FTIR** (KBr pill, cm^{-1}): 3265 (NH), 3060 (C–H aromatic), 1477 (P–Ar), 1218 and 1142 (P=O), 1043 (P–O–C), 914 (P–O-Ar), 753. **^{1}H-NMR** (400 MHz, DMSO-d6, d, ppm): 8.50 (m, 2H), 8.17 (m, 4H), 7.88 (m, 2H), 7.68 (m, 2H), 7.56 (m, 2H), 7.42 (m, 2H), 7.34 (m, 4H), 7.18 (m, 2H), 6.54 (m, 8H), 6.1 and 5.6 (m, 2H, N–H), 5.4 and 4.9 (m, 2H, CH–P).

1.3.2. Synthesis and structural characterization of the OP

The OP was obtained by solution polycondensation reaction of equimolar amount of the precursor with phenylphosphonic dichloride (Scheme 1). In a flask equipped with a reflux condenser, magnetical stirrer and nitrogen inlet and outlet, were introduced and mixed the precursor (7.48 g, 0.01 mol), N-methyl-2-pyrrolidone (NMP) (30 mL) and triethylamine (3 mL). After a homogeneous solution was obtained phenylphosphonic dichloride (1.95 g, 0.01 mol) was added under stirring, during 0.5 h. The reaction flask was then immersed in an oil bath at 50 °C and the mixture was stirred vigorously for 8 h. The resulting solution was then cooled to room temperature and poured into methanol. The obtained solid was filtered and re-dissolved in NMP. The oligomer was isolated by precipitation in water, washed several times with water, and dried at 60 °C in a vacuum oven for 24 h to give a powdery solid (yield: 94%).
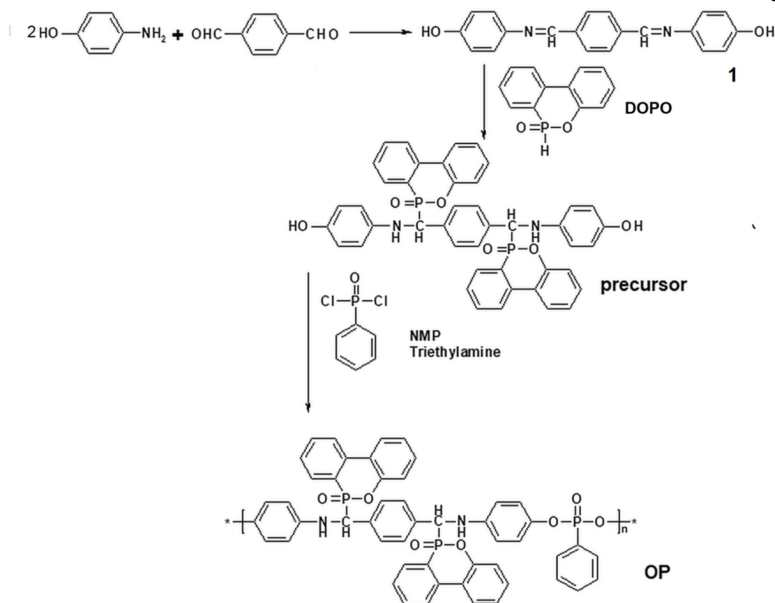
Scheme 1. The synthesis of the precursor to the OP and the OP.
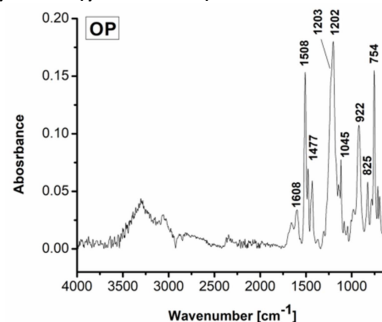
Figure 1. FTIR spectrum of the OP.
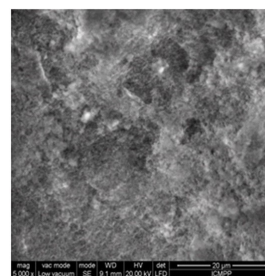
Figure 2. SEM micrograph of the OP.

Characterization of the OP

Structural characterization of the OP was investigated by **FTIR** spectroscopy (Figure 1). The OP component exhibited a sharp absorption band at 1477 cm^{-1}, describing the aromatic P–C stretching vibrations. The bands from 1202 and 922 cm^{-1} correspond to aromatic P–O–C stretching vibrations. The band at 1045 cm^{-1} was attributed to the aliphatic P–O–C bond asymmetric stretching vibrations. The band at 1203 cm^{-1} corresponds to aromatic P=O stretching. The deformation vibrations of 1,2–disubstituted aromatic DOPO rings generate the band at 754 cm^{-1}, while the band at 825 cm^{-1} is characteristic to the deformation vibrations of p–phenylene rings. The signals at 1608 and 1508 cm^{-1} correspond to aromatic C=C stretching vibrations. *Morphological characterization* of the OP by **SEM** is shown in Figure 2. The OP

possesses high solubility in polar aprotic solvents: dimethylformamide (DMF), *N,N*–dimethylacetamide and NMP. This good solubility is induced by the presence of bulky pendant DOPO entities in the diol increasing the free interchain volume and enhancing solvent diffusion in the macromolecules. Through the gel permeation chromatography **(GPC)** method the molecular weights and distribution were determined for the OP. The number average molecular weight (M_n) was 6184 g mol^{-1} and the weight average molecular weight (M_w) was 6501 g mol^{-1}. The polydispersity (M_w/M_n) was 1.051. The GPC curve showed a narrow molecular weight distribution. The relatively low molecular weight values are a consequence of the bulky DOPO entities decreasing functional group reactivity and hindering polycondensation propagation. **The inherent viscosity** was determined at a concentration of 0.5 % (w/v) OP solution in 1–methyl–2–pyrrolidone (NMP) at 25 ^{o}C on an Ubbelohde viscometer and was found to be 0.95 cL g^{-1}, characteristic to low molecular weight polymers.

Stage 2. **The obtaining and characterization of the S–IPNs based on OP and epoxy resin (continuation from Stage 1). The thermal and fire behavior of the S–IPNs.**
Activity 2.1. The obtaining and characterization of the S–IPNs based on OP and an epoxy resin
2.1.1. Obtaining and characterizaton of the S–IPNs
The S–IPNs were obtained by mixing the epoxy resin, diglycidyl ether of bisphenol A (EP) with different amounts of OP under heating and stirring, followed by the curing in the presence of a suitable hardener (Table 1). The OP was previously synthesized and described in Stage 1 (2020 – Activity 1.3). 4,4'–diaminodiphenylsulfone (DDS), 1,3–bis(aminomethyl)cyclohexane (CYDM) and octamethylenediamine (8CH$_2$DA) were used as curing agents for the epoxy resin to obtain three S–INPs (Scheme 2). The epoxy to amine ratio was set at 2:1 based on the assumption that each hydrogen atom on the nitrogen atoms from the curing agents reacts with an epoxide ring. The quantity of OP was calculated in order to obtain final products with 2 wt% phosphorus. The various formulations of the pre–curing mixtures are listed in Table 1. The required quantities of epoxy resin were mixed with OP under continuous stirring at 130 ^{o}C until complete dissolution was achieved followed by the addition of a hardener and cooling of the mixture to 80 ^{o}C. The resulting mixtures were stirred homogeneously and poured into a Teflon coated mould to obtain the samples in the shape of plates. The formulation based on DDS was cured at 150 ^{o}C for 2 h and 180 ^{o}C for 3 h. The rest of the samples were cured at 70 ^{o}C for 4 h, 130 ^{o}C for 2 h and 150 ^{o}C for 1 h. Finally, the thermosets were cooled slowly to room temperature to prevent cracking.
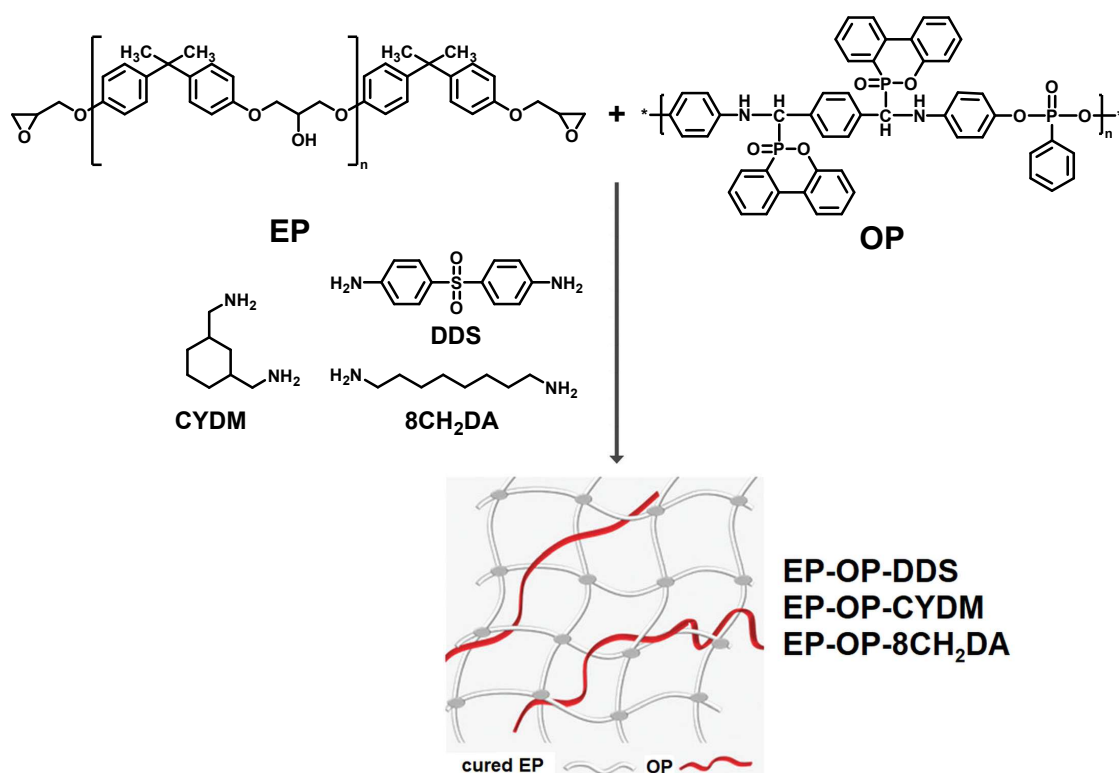
Scheme 2. Obtaining of the cured matrices and S–IPNs.

Table 1. Composition of the samples.

Sample	Hardener	Hardener (g)	Oligophosphonate (OP) (g)	Epoxy resin (EP) (g)
EP–DDS	DDS	7.45	-	22.55
EP–OP–DDS	DDS	5.99	5.61	18.36
EP–CYDM	CYDM	4.66	-	25.34
EP–OP–CYDM	CYDM	3.79	5.56	20.63
EP–8CH$_2$DA	8CH$_2$DA	4.79	-	25.23
EP–OP–8CH$_2$DA	8CH$_2$DA	3.87	5.65	20.50

where: EP–OP–DDS, EP–OP–CYDM and EP–OP–8CH$_2$DA are the S–IPNs and EP–DDS, EP–CYDM and EP–8CH$_2$DA the cured matrices without the OP

The structural investigations of the S–IPNs were undertaken by FTIR and SEM-EDX techniques.

FTIR: The FTIR spectra of the S–IPNs are given in Figure 3a. The OP component exhibited a sharp absorption band at 1477 cm^{-1} describing the aromatic P–C stretching vibrations. The bands from 1202, 1045 and 922 cm^{-1} correspond to P–O–C stretching vibrations. According to the literature the weak signals region 1040–910 cm^{-1} of the samples spectra describe stretching vibrations of P–OH bond in O=P–OH from the end–capping of the low content OP in the networks [1]. The band at 1203 cm^{-1} corresponds to aromatic P=O stretching. The deformation vibrations of 1,2–disubstituted aromatic DOPO rings generate the band at 754 cm^{-1}, while the band at 825 cm^{-1} is characteristic to the deformation vibrations of p–phenylene rings [2]. The signals at 1608 and 1508 cm^{-1} correspond to aromatic C=C stretching vibrations.
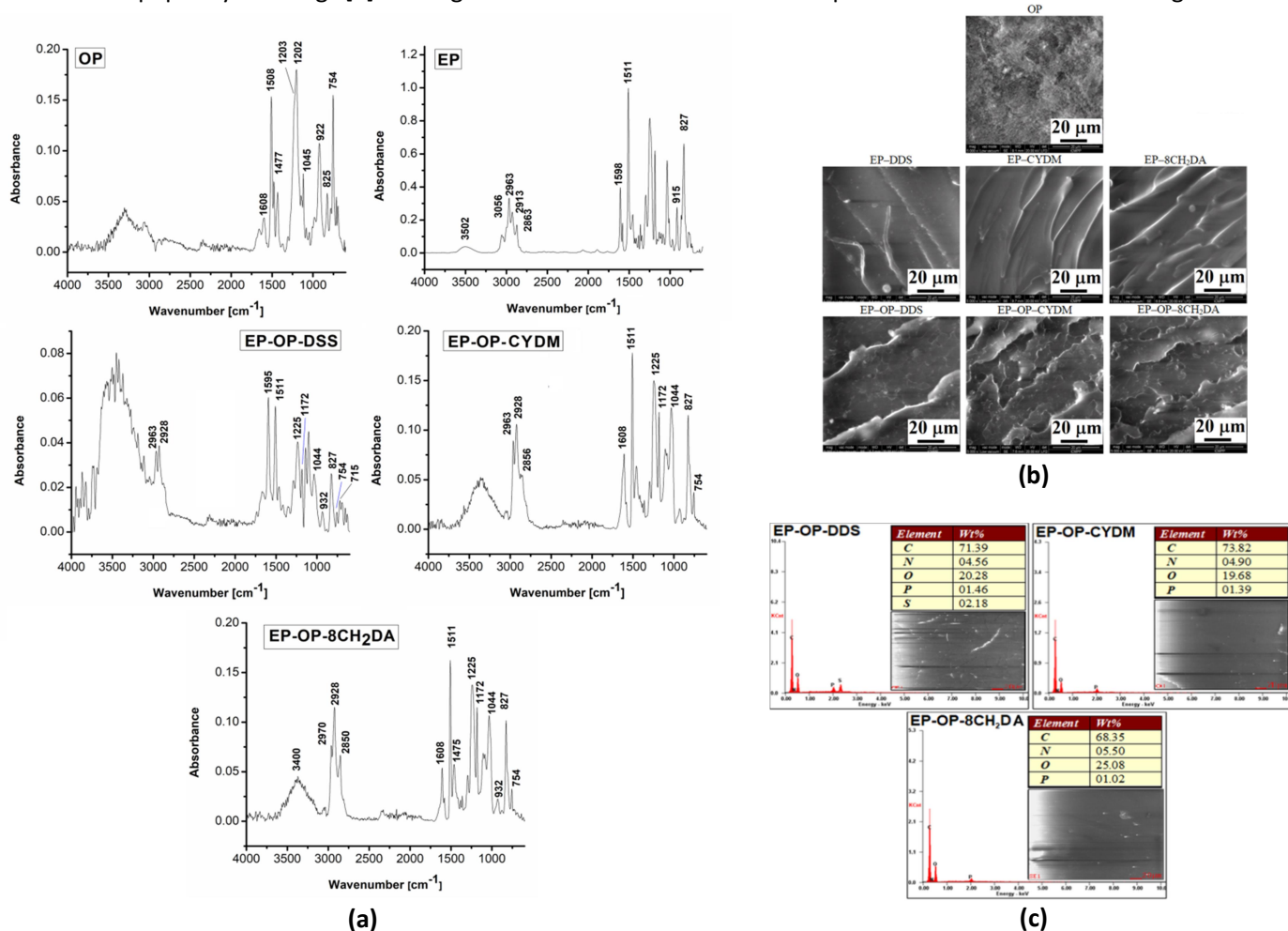
Figure 3. FTIR spectra (a), SEM micrographs (b) and EDX analysis (c) of the S–IPNs.

The epoxy resin is mainly characterized by the signal localized at 915 cm^{-1} specific to the epoxy ring and the signals from 1598 and 1511 cm^{-1} characteristic to skeletal C=C vibrations in aromatic moieties. In addition, the region 1000–

1300 cm^{-1} describes aryl alkyl ether moieties [3]. These signals also appear in the FTIR spectra of the S–IPNs. The group of signals around 2963 cm^{-1} and 2928 cm^{-1} correspond to aliphatic C–H asymmetric stretching vibrations, while the one around 2850 cm^{-1} is attributed to aliphatic C–H symmetric stretching vibrations. The broad band around 3502 cm^{-1} in the FTIR spectrum of EP corresponds to O–H stretching vibrations. Upon curing the epoxy matrices, the epoxide ring is cleaved resulting more O–H entities and N–H stretching vibrations appear from secondary amines. Thus, the region 3000–4000 cm^{-1} (with a peak at around 3400 cm^{-1}) becomes much broader and intense in FTIR spectra of the S–IPNs, as one may see in Figure 3. The opening of the epoxy ring was further confirmed by the absence of its characteristic absorption bands in the S–IPNs spectra: the band at 3056 cm^{-1} (C–H stretching vibrations of methylene from the epoxy ring) and the band located at 915 cm^{-1}. Furthermore, the bands at 1172 and at 1225 cm^{-1} correspond to the secondary amines, demonstrating the formation of C–N bonds after the epoxide ring opening with the diamines [2]. The S–IPNs exhibited important signals, such as the one at 1475 cm^{-1}, corresponding to stretching vibrations of aromatic P–C bond. The signals at 1044 cm^{-1} and 932 cm^{-1} are attributed to P–O–C bond stretching vibrations. The signals at 754 and 715 cm^{-1} are due to deformation vibrations of the 1,2–disubstituted aromatic DOPO and aromatic rings of the DDS curing agent in EP–OP–DDS. The presence of all these signals successfully confirms the obtaining of the S–IPNs [1].

SEM–EDX: Figure 3b shows the SEM micrographs of the samples fracture surfaces obtained after cooling in liquid nitrogen. The micro fractures are spread within the entire S–IPNs sample masses, the minimal fracture area occurring through crack propagation. The uniform fractures were generated during thermal treatment by OP agglomerates, behaving as stress concentration centers and indicating a good homogeneous dispersion of the OP into the cured epoxy matrices [4]. Moreover, the reactive epoxide rings of the resin are crosslinked to generate larger chains, indicating that the curing agents are well distributed within the whole matrix. The EDX analysis confirmed the presence of low content phosphorous from OP in the S–IPNs (Figure 3c).

Activity 2.2. The microbiological testing of the S–IPNs

Since the S–IPNs are intended as future wood protective coatings, the samples microbiological resistance was tested against three wood decaying fungal strains: *Penicillium chrysogenum* ATCC10106, *Cladosporium cladosporioides* ATCC16022 and *Aspergillus brasiliensis* ATCC 9642. In our case, the assessment of degradation degree after 10 weeks of exposure was based on visual observations. As it may be observed from Figures 4, during the decay test all surfaces of samples were not covered by the fungal colonies, except samples exposed to *A. brasiliensis* where the edges where slightly covered.
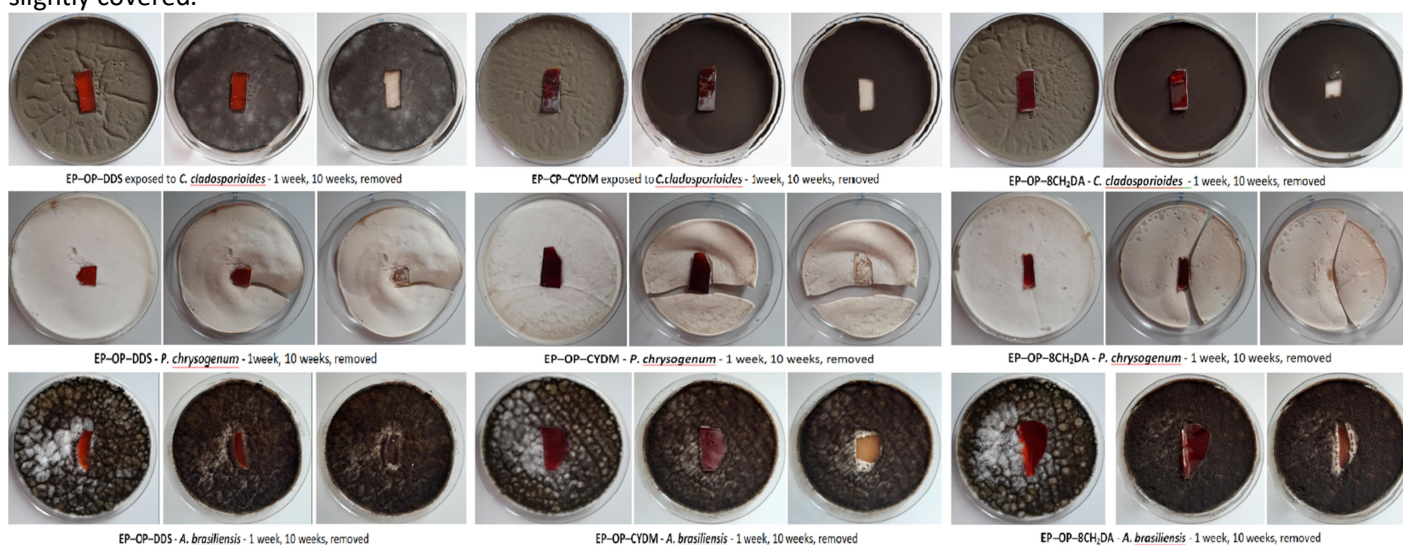
Figure 4. Microbiological testing of the networks.

Even if there was not distinguished a notable growth of the colonies on the samples, the fungistatic properties when compared with a control varied (Figures 4). The sample encoded EP–OP–CYDM reduced the population of *P. chrysogenum* at 17 %. Not so promising results were obtained in case of the samples incubated with *A. brasiliensis*, where there was not noticed a fungistatic activity for none of the tested samples. Also it was noticed that the S–IPNs had a greater fungistatic activity than their cured counterparts without OP, due to the presence of phosphorus. The samples presented instead fungicidal properties when incubated with *C. cladosporioides* and *A. brasiliensis* and partially for *P. chrysogenum*, the areas under the samples remaining clear of fungal colonies after 10 weeks of incubation where the samples adhered perfectly to the culture media (Figures 4).
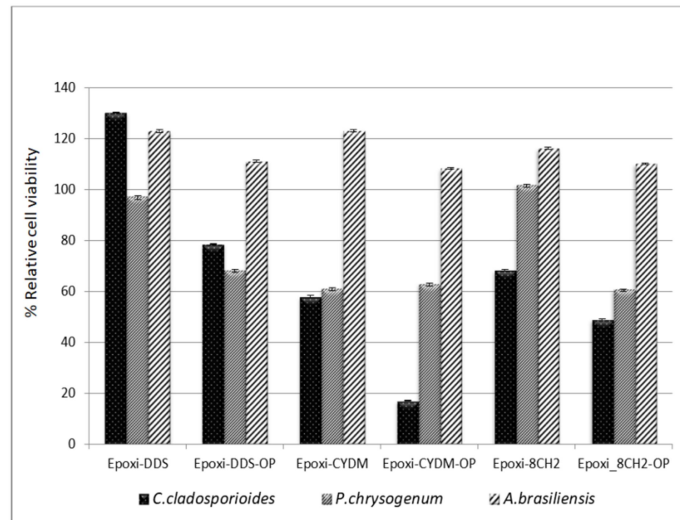
Figure 4. Microbiological testing of the networks.

Activity 2.3. The thermal and fire behavior of the S–IPNs

2.3.1. DSC and comparative thermal degradation studies in inert and thermo–oxidative atmospheres by TGA

2.3.1.1. DSC study

Assessment of thermal stability of materials for high temperature applications is crucial and resides in the evaluation of some essential parameters: the temperature corresponding to 5 % mass loss ($T_{5\%}$), the temperature at which the mass loss rate is the highest (T_{max}), mass residue remaining after thermal degradation (700 $^{\circ}$C) and the glass transition temperature (T_g). The thermal behavior of the S–IPNs, OP and crosslinked epoxy matrices was evaluated. All structures exhibited a single neat T_g domain (Figure 5). The OP showed a T_g value at 132 $^{\circ}$C. No other thermal transitions were observed, hence no further crosslinking expected to occur. The presence of a single T_g domain is a sign of good compatibility between components within the S–IPNs. It is a known fact that the obtaining of S–IPNs induces a forced phase compatibilization through a synergistic effect of the comprising components, based on compatible polarities [5]. One may also observe from the DSC data that the T_g values of the S–IPNs are situated between those of the OP and their corresponding cured matrices. This is an indication that the S–IPNs were successfully obtained [5]. The bulky aromatic DOPO entities in OP generate a steric hindering effect, leading to an increase in S–IPNs T_g values compared to their corresponding crosslinked epoxy matrices, except for the sample cured with DDS. In this case, the presence of OP had a strong plasticizing effect which led to a significant reduction in the T_g value from 201 $^{\circ}$C (EP–DDS) to 141 $^{\circ}$C (EP–OP–DDS). This is due to the increase in free volume between segmental chains and hence their mobility, which is also dictated by the bulky aromatic nature of the curing agent, as also found for other S–IPN epoxy systems, making the material adequate for applications which require lower T_g values [4].
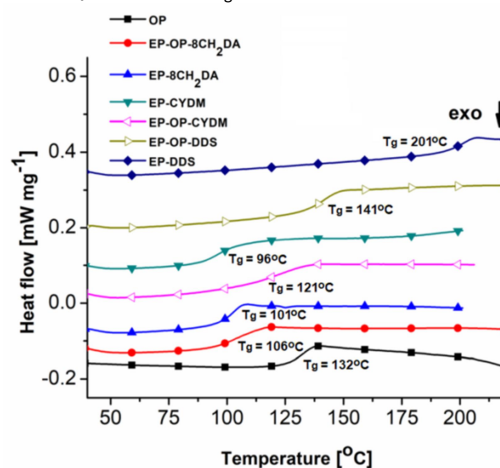
Figure 5. DSC curves of the OP and networks.

2.3.1.2. TGA studies in inert and thermo–oxidative atmospheres

The phosphorus influence on the thermal stability of the structures was investigated with the aid of TGA and first derivative curves (DTG) in both inert and air atmospheres. The main data extracted from the thermal measurements are shown in Figure 6 and Table 2. In both atmospheres the individual linear component, OP, underwent a complex thermal decomposition process in four overlapping stages. In an inert atmosphere (N_2), the OP exhibited a 5 % mass loss temperature ($T_{5\%}$) value of 275 ^oC and a multi–step decomposition pattern with maximum decomposition temperature (T_{max}) values of 311 ^oC, 395 ^oC, 430 ^oC, 491 ^oC, a thermal degradation endset temperature (T_{endset}) of 530 ^oC and a final stable residue (R) of 55.5 %. As expected, the presence of oxygen accelerated the thermal degradation of the OP in air, resulting in lower characteristic temperatures ($T_{5\%}$ = 258 ^oC; T_{max} = 297 ^oC, 372 ^oC, 418 ^oC, 485 ^oC; T_{endset} = 510 ^oC) and R value (43.28 %).

In nitrogen atmosphere the aromatic nature of the DDS curing agent endowed the crosslinked epoxide matrix (EP–DDS) with the highest thermal stability of all the investigated materials ($T_{5\%}$ = 381 ^oC), decomposing in a single stage (T_{max} = 410 ^oC) and yielding 21.21 % residue. By comparison to EP–DDS, the cycloaliphatic and aliphatic hardeners exhibited additional thermal decomposition (overlapping) stages and decreased thermal stability. The corresponding cured epoxy matrices (EP–CYDM, EP–8CH$_2$DA), exhibit $T_{5\%}$ = 352 ^oC and lower almost identical residues of 9.75 % (EP–CYDM) and 9.25 % (EP–8CH$_2$DA), respectively. The TGA residues increased for OP containing S–IPNs to 34 % for EP–OP–DDS, 12.26 % for EP–OP–CYDM and 13.04 % for EP–OP–8CH$_2$DA. The increased char formation of OP blocks the release of volatile products due to the solid phase action of the phosphorus. The S–IPNs thermal stabilities were also dictated by the chemistry of the curing agent (EP–OP–DDS > EP–OP–CYDM > EP–OP–8CH$_2$DA). The S–IPNs containing OP exhibit lower $T_{5\%}$ values which could be due to catalyzed decomposition caused by phosphorus based acidic species. In addition, during the formation of the S–IPNs there occur hydrogen bonds disruptions in both the OP and epoxy resin when the OP gets trapped within the crosslinked epoxy network during curing. This aspect, together with the lower thermal stability of OP, due to the more thermally labile P–C bond in the additive, leads to the decrease of $T_{5\%}$ in the S–IPNs below that of the neat OP. Rosu et al. [6] correlated the broadening of the $T_{endset} - T_{5\%}$ range with surface compactness during thermal degradation leading to decrease in volatiles evolvement. The same is observed in the case of this study. The obtained S–IPNs are more compact than their comprising components, because a decrease in the rate of volatiles evolvement due to the significant broadening of the range $T_{endset} - T_{5\%}$ of the S–IPNs by comparison to their crosslinked matrices without OP (Table 2). The TGA measurements undertaken in air showed that the presence of oxygen led to a more complex degradation mechanism of the epoxy samples. This explains the very high differences in char yield between the two working atmospheres, in air being lower. Regardless of the working atmosphere, the $T_{5\%}$ and T_{max} values of S–IPNs were generally lower than those of the cured epoxy matrices, due to the lower thermal resistance of the P–C bond [7].
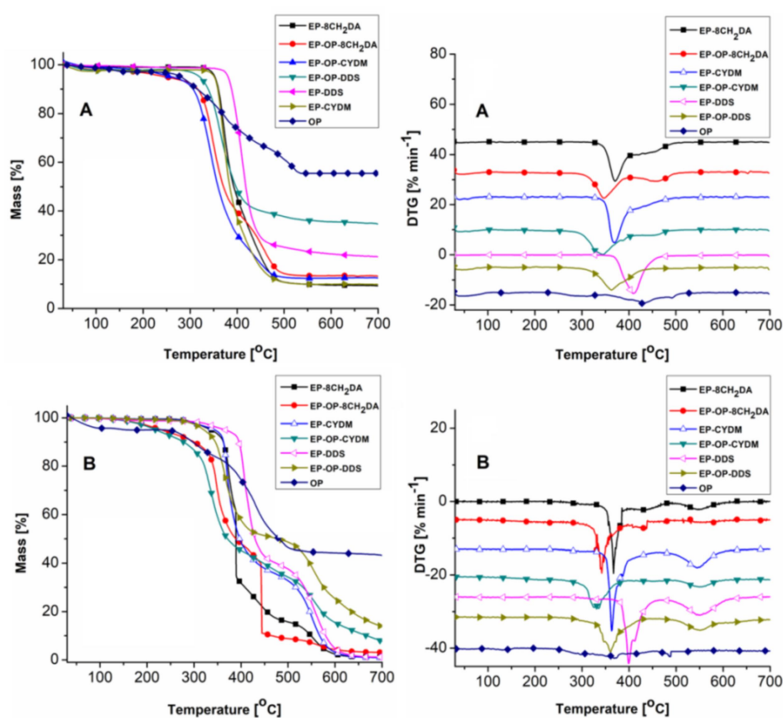
Figure 6. TGA (left) and DTG curves (right) in (A) nitrogen and (B) air.

Table 2. Thermal properties of the structures.

| Sample | Atm. | $T_{5\%}$ (°C) | Thermal degradation stages | | | | T_{endset} (°C) | $T_{endset} - T_{5\%}$ (°C) | R (%) | T_g (°C) |
			T_{max1} (°C)	T_{max2} (°C)	T_{max3} (°C)	T_{max4} (°C)				
OP	Air	258	297	372	418	485	510	252	43.28	–
	N_2	275	311	395	430	491	530	255	55.5	132
EP–DDS	Air	359	400	550	–	–	600	241	1.25	–
	N_2	381	410	–	–	–	450	69	21.21	201
EP–OP–DDS	Air	315	360	550	–	–	575	260	13.31	–
	N_2	321	363	387	–	–	410	89	34	141
EP–CYDM	Air	339	364	546	–	–	590	251	1.02	–
	N_2	352	370	437	–	–	460	108	9.75	96
EP–OP–CYDM	Air	213	335	552	–	–	580	367	7.13	–
	N_2	262	344	387	458	–	473	201	12.26	121
EP–8CH₂DA	Air	330	300	370	550	–	590	260	1.11	–
	N_2	352	371	435	–	–	475	123	9.26	101
EP–OP–8CH₂DA	Air	225	340	435	555	–	587	362	3.07	–
	N_2	249	347	462	–	–	485	236	13.04	106

$T_{5\%}$ – temperature corresponding to 5 % mass loss;
T_{max} – temperature corresponding to the highest mass loss rate per each thermal degradation stage;
T_{endset} – temperature corresponding to the endset of thermal degradation;
R – residue mass remained at 700 °C;
T_g – glass transition temperature.

2.3.2. Determination of non–isothermal kinetic parameters of thermal degradation

The undertaking of the thermal kinetic studies was in accordance with the recommendations of the International Confederation on Thermal Analysis and Calorimetry (ICTAC) [8]. In Figure 7 there are shown the TGA and DTG curves registered at 10, 20, 30 °C min⁻¹ heating rates under nitrogen atmosphere for the S–IPNs. Using the TGA curves at three heating rates and the Friedman (FR) and Ozawa–Flynn–Wall (OFW) equations included in the "Netzsch Thermokinetics-3" software the initial kinetic thermal degradation parameters were calculated. Figure 7 shows that with the increase of the heating rate, the TG curves shift to higher temperatures due to temperature delay as a function of heating rate [9,10]. The data in Tables 2 and 3, the DTG curve shapes and the variation of activation energy (E_a) with the conversion degree (α) (Figure 8) show that the degradation processes follow complex mechanisms in multiple reactions: consecutive, parallel or competitive [11,12].

The fact that the degradation processes are complex requires the use of the multiple linear regression (MLR) method to identify the degradation mechanisms. MLR assumes that the parameters of the kinetic model are identical for all measurements. Using an iterative method, the software numerically resolves the differential equations of some reaction models (18 reaction mechanisms) [13,14] for α in the range 0.1 – 0.85, calculating the minimum value of least squares between simulated and the experimental data, suggesting the best kinetic model for the thermal degradation process. The most probable kinetic model was chosen based on visual appreciation and of statistics coefficients (the experimental F–value ((Fexp), Fcrit (0.95) and correlation coefficients). In the present case the successive processes take place in two and three steps and were assigned to the schemes (1) and (2) (Table 3):

$$A\text{-}1 \rightarrow B\text{-}2 \rightarrow C \tag{1}$$
$$A\text{-}1 \rightarrow B\text{-}2 \rightarrow C\text{-}3 \rightarrow D \tag{2}$$

with the following types of process mechanisms: d:f; An,Fn, for EP–OP–8CH₂DA and EP–OP–DDS and t:f,f; An, Fn, Fn for EP–OP–CYDM. A is the solid initial product, B is the intermediate products (solid, liquid or gaseous) and C/ D is the final solid residue. The numbers 1, 2, 3 represent the reaction steps.

The next conversion functions for one single step were used:

-Avrami–Erofeev reaction model An: $\quad f(\alpha) = n(1 - \alpha)[-\ln(1 - \alpha)]$ (3)

where n is a constant parameter.

- nth reaction order model Fn: $\quad f(\alpha) = (1 - \alpha)^n$ (4)

where n is the reaction order and α is the conversion degree;

Using the kinetic parameters presented in Table 3, the TGA curves can be recalculated (between 200 and 550 $^{\circ}$C). These recalculated curves approximate well the experimental data, suggesting that the obtained theoretical models accurately simulate the real thermal degradation phenomenon (Figure 7).

As seen in Table 3, for all samples, in the majority of degradation stages the reaction order has values greater than 1 [15].

E_a and the pre–exponential factor (logA) differ depending on the chemical structure of the curing agents. The activation energies vary between 190 and 250 kJ mol^{-1} for the samples cured with aliphatic hardeners and between 219 and 242 kJ mol^{-1} for the sample cured with aromatic hardener. The total E_a assigned to the entire thermal decomposition process is the sum of the E_a values for each step.
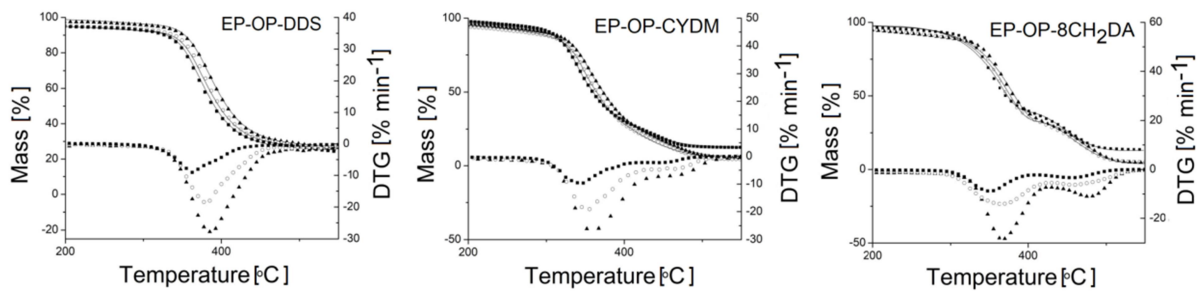
Figure 7. TG and DTG curves registered at: (■) 10, (○) 20, (▲) 30 $^{\circ}$C min^{-1} heating rates. The continuous line represents experimental curves. Symbols represent software simulated curves.
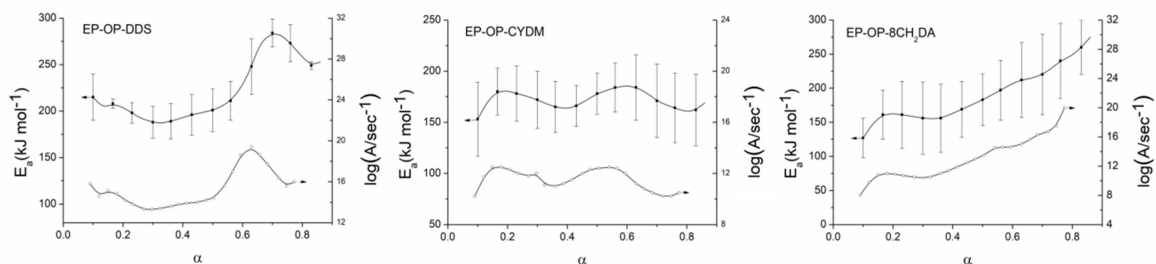
Figure 8. Variation of kinetic parameters with conversion degree.

Table 3. Kinetic and statistics parameters determined after non-linear regression for the most probable mechanism of thermal degradation process of the S–IPNs products by applying a kinetic model in two and three steps, with consecutive reactions in the temperature interval 100–550 $^{\circ}$C.

Parameters	EP–OP–DDS	EP–OP–CYDM	EP–OP–8CH$_2$DA
	d:f; An,Fn	t:f,f; An,Fn,Fn	d:f; An,Fn
	mechanism scheme	mechanism scheme	mechanism scheme
	A-1→B-2→C	A-1→B-2→C-3→D	A-1→B-2→C
E_1 /kJmol^{-1}	242	196	221
log A_1/s^{-1}	15.85	14.03	20.76
n_1	0.338	0.215	0.245
E_2 /kJmol^{-1}	219	219	190
log A_2/s^{-1}	16.17	16.45	14.03
n_2	2.661	0.973	3.536
E_3 /kJmol^{-1}	-	250	-
log A_3/s^{-1}	-	19.89	-
n_3	-	1.384	-
follReact 1	0.8245	0.216	0.112
follReact 2	-	0.690	-
Fexp	1.00	1.00	1.00
Fcrit-0.95.	1.19	1.16	1.196
t-critical(0.95)	1.956	1.956	1.956
correl-coeff	0.999017	0.999883	0.999527

E_1, E_2, E_3 – represent the activation energies of thermal degradation for each step; log (A_1, A_2, A_3) are the pre-exponential factors for each step; n_1, n_2, n_3 are the reaction order for each step; logKcat1 is the autocatalytic constant for the reaction step 1; follReact 1 is the share from the total process for the reaction step 1 (A→B); follReact 2 is the share from the total process for the reaction step 2 (B→C) and the share of step 3 (C→D) in the total process, is given by $1 - \sum (\text{follReact})$

2.3.3. Evolved gases analyses by TGA–FTIR and Py–GC–MS

2.3.3.1. TGA–FTIR

TGA–FTIR coupling was used to study the evolved gaseous mixtures formed during the thermal degradation of the epoxy samples. The FTIR spectra of volatiles released from the decomposition of OP and S–IPNs at relevant T_{max} values (Table 2) are presented in Figure 9. The weak signal at 3059 cm^{-1} in the FTIR spectra for OP is associated with the aromatic C–H stretching vibration, as well as the signal 3011–3016 cm^{-1} are found in all spectra [16]. The peaks at 3086 cm^{-1} and 3113 cm^{-1} correspond to N–H from amine moieties. The broad signal in the range 3500–3000 cm^{-1} with a peak at ~3250 cm^{-1}, present in all spectra, corresponds to O–H bond stretching vibrations of alcohol moieties and/or carboxylic acids. Signals corresponding to aliphatic C–H asymmetric and symmetric stretching vibrations observed (~2959 cm^{-1} and ~2937 cm^{-1}) could be due to different moieties, including fractions containing CH$_3$. The signals from 1500–1600 cm^{-1} and 690–669 cm^{-1} confirm the presence of entities with aromatic structures. The peak at around ~2360 cm^{-1} also appears in all spectra and is ascribed to CO$_2$ evolution, together with the range 4000–3500 cm^{-1}, associated with water. The signals in the range 1200–2000 cm^{-1} contain overlapping absorption bands from: vibrations of C=O, C=C, water, cycloaliphatic structures, P–Ar stretching vibrations (~1420 cm^{-1}), P=O stretching vibrations (~1185 cm^{-1}), ketone stretching vibrations (~1690–1747 cm^{-1}). The decarboxylation reaction and scission of the different carbonyl groups lead to the formation of CO$_2$. Additional bands at around 1600 and 1509 cm^{-1} correspond to C=C stretching vibration of aromatic rings. The absorption bands around 3000 cm^{-1} describe the sp^2 and sp^3 C–H stretching vibrations of aromatic and aliphatic species.
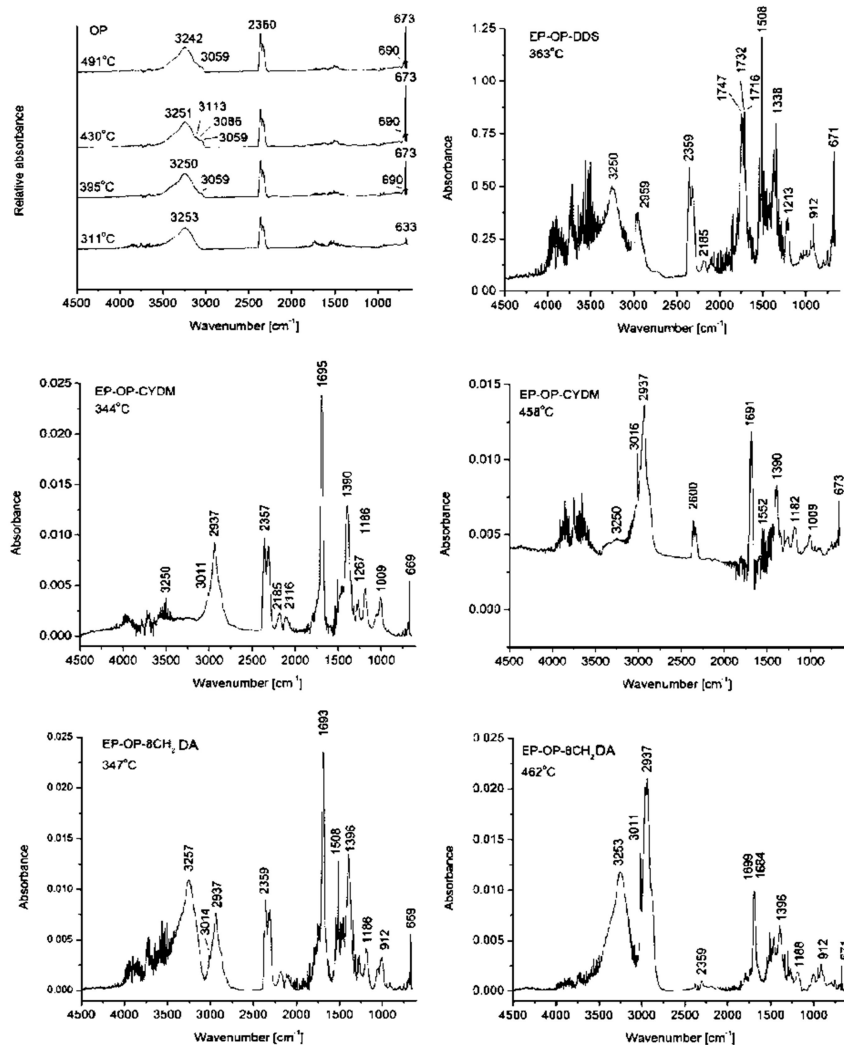
Figure 9. Gaseous FTIR spectra of the structures extracted from T_{max} values.

2.3.3.2. Py–GC–MS

The FTIR spectra offer information only concerning functional groups of the gaseous entities evolved during the decomposition of the polymer. Therefore, gas chromatography (GC) coupled with mass spectroscopy (MS) was used to identify the composition of pyrolysis (Py) products (Py–GC–MS). Figure 10 presents the Py–GC–MS total ion chromatograms and Table 4 shows the main identified evolved gaseous products of the S–IPNs and OP pyrolyzed at 600 ^{o}C, where +/ – denote a present/absent gaseous entity in a compound. Based on the data in Figure 10 and Table 4, a simplified thermal degradation mechanism for the S–IPNs (EP–OP–CYDM, as an exemplification) was proposed in Scheme 3. The NIST mass spectral database and prior published literature were used to identify the pyrolyzates from their mass spectra and retention times. By analyzing the total ion chromatogram (TIC) of the OP one may observe a series of pyrolyzates identified at different retention times (RT). This aspect indicates the presence of a complex gaseous mixture evolved during the OP and S–IPNs decomposition, comprised of: p–xylene (RT = 2.74 min; m/z = 91; abundance (a) = 5.47 x 10^{5}); aniline (RT = 3.46 min; m/z = 93, 92, 66, 65; a = 1.21 x 10^{6}) + phenol + phenyl phosphonic acid (RT = 3.59 min; m/z = 94, 92, 66, 65; 174, 94, 66, 9; a = 4.1 x 10^{5}) and N–methyl–1–pyrrolidone as solvent (NMP) (RT = 3.88 min; m/z = 99, 98, 44, 42, 41; a = 3.42 x 10^{6}). As observed, the predominantly aromatic structure of OP generated mostly aromatic pyrolyzates upon degradation, such as p–aminophenol, biphenyl (RT = 5.93 min; m/z = 154, 153, 152; a = 4.9 x 10^{5}) and 2–phenylphenol (RT = 6.64 min; m/z = 170, 169, 167, 141, 115; a = 1.44 x 10^{6}). Phenyl phosphonic acid also originates from the OP, since it is the sole compound containing phosphorus. The peak of phenyl phosphonic acid is partially merged with the high peak corresponding to phenol. Phenyl phosphonic acid may be generated through cleavage of the Ar–O bond in the OP main chain, hydrogen atoms and hydroxyl groups transfer. P–aminophenol, biphenyl and 2–phenylphenol appear at higher temperatures (higher RTs) [17]. The gaseous fragments specific to the OP, mostly phenols, do not appear in the case of the S–IPNs. This is in good agreement with the TGA data where the decrease in rate of volatiles formation (increased char formation) was observed, due to the compactness of the S–IPNs by the significant broadening of the T_{endset} – $T_{5\%}$ range. The common gaseous fragments evolved during the thermal degradation of the S–IPNs correspond well with the components of epoxy resin, while the slight differences between the samples may arise from the structures of the curing agents. Literature data shows that bisphenol A and aromatic amines are formed during the thermal decomposition of epoxy resins crosslinked with aromatic amine hardeners [18,19].

Table 4. Main pyrolysis products identification.

No.	Retention time (min)	Name	Mass	Ions (m/z)	Structure	EP-OP-DDS	EP-OP-CYDM	EP-OP-8CH$_2$DA	OP
1	2.73–3	p–xylene (pX)	91	91		+	+	+	+
2	3.46-3.61	aniline (An)	93	93; 92; 66; 65		+	+	+	+
3		phenol (P)	94	94; 93; 66; 92; 65;		+	+	+	+
4		phenyl phosphonic acid (pHpPA)	158	158		+	+	+	+
5	3.88-3.98	N-methyl-1- pyrrolidone (NMP)	99	99; 98; 44; 42; 41		+	+	+	+
6	3.97-3.99	4-methylphenol (4MPh)	108	108; 107		+	+	+	–
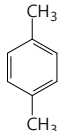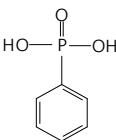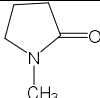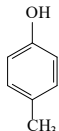
7	5.02-5.05	4-(1-methylethyl)phenol (4-1MEPh)	136	121; 136		+	+	+	−
8	5.47	p-isopropenylphenol (pIpPh)	134	134; 119; 91		+	−	−	−
9	5.36+5.40	p–aminophenol (pAPh)	109	109		−	−	−	+
10	5.93	biphenyl (bP)	154	154; 153; 152		−	−	−	+
11	6.64	2-phenylphenol (2PPh)	170	170; 169; 167; 141; 115		−	−	−	+
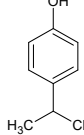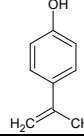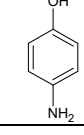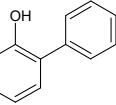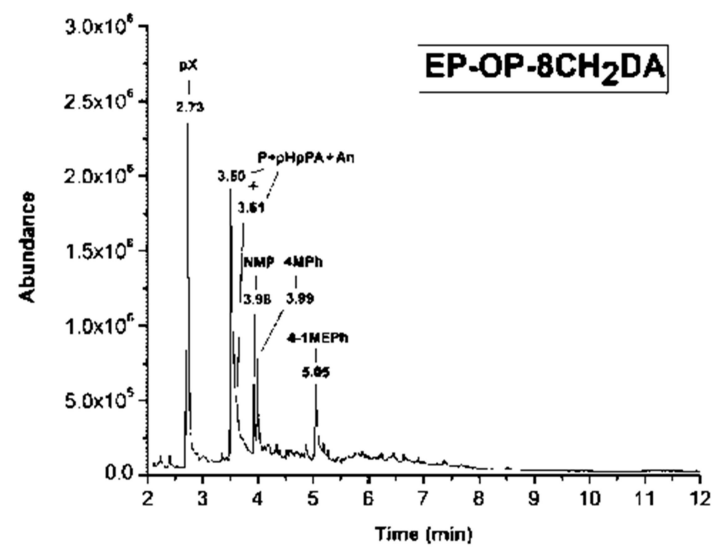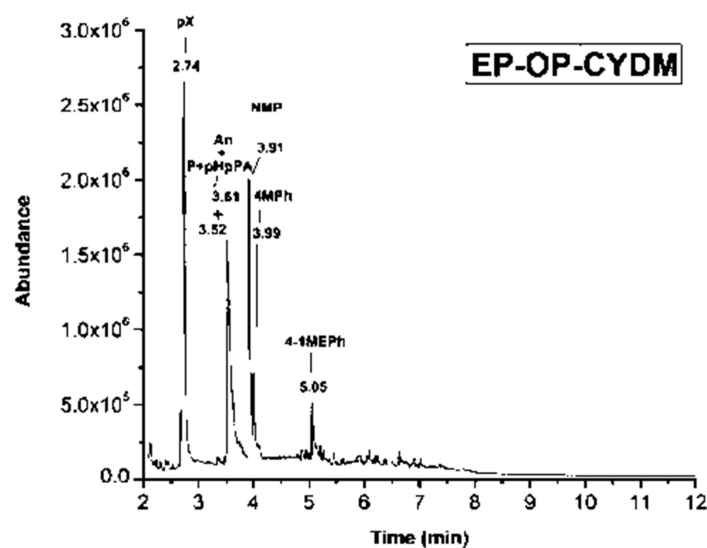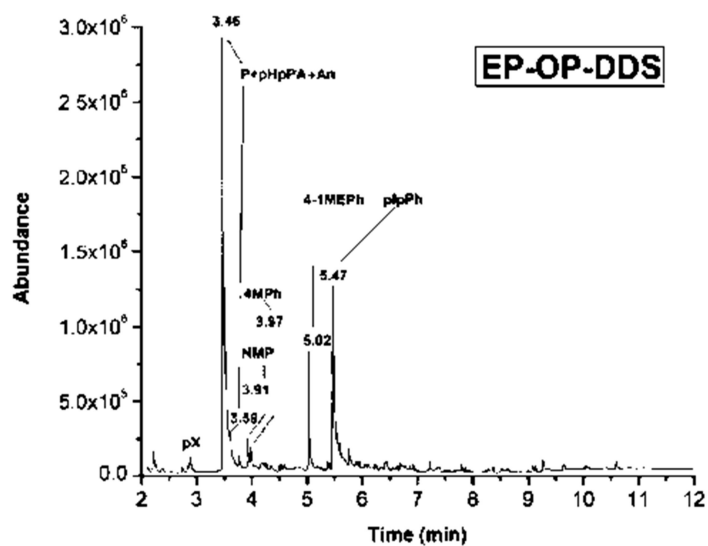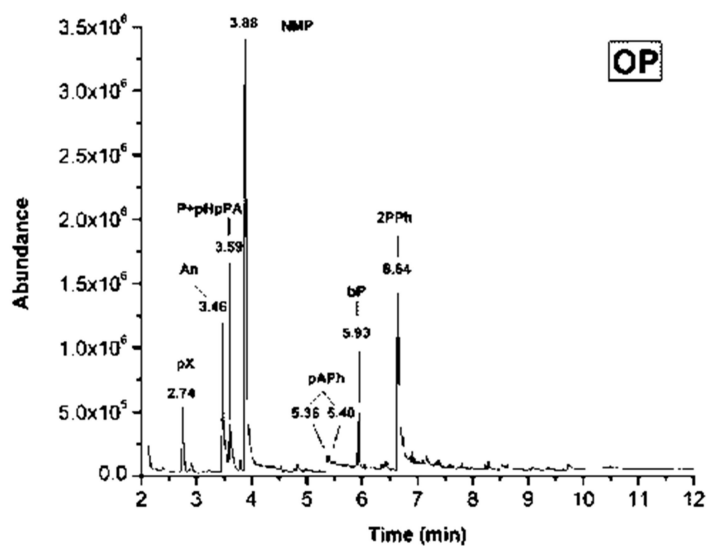
Figure 10. The total ion chromatograms of the S–IPNs recorded at 600°C.
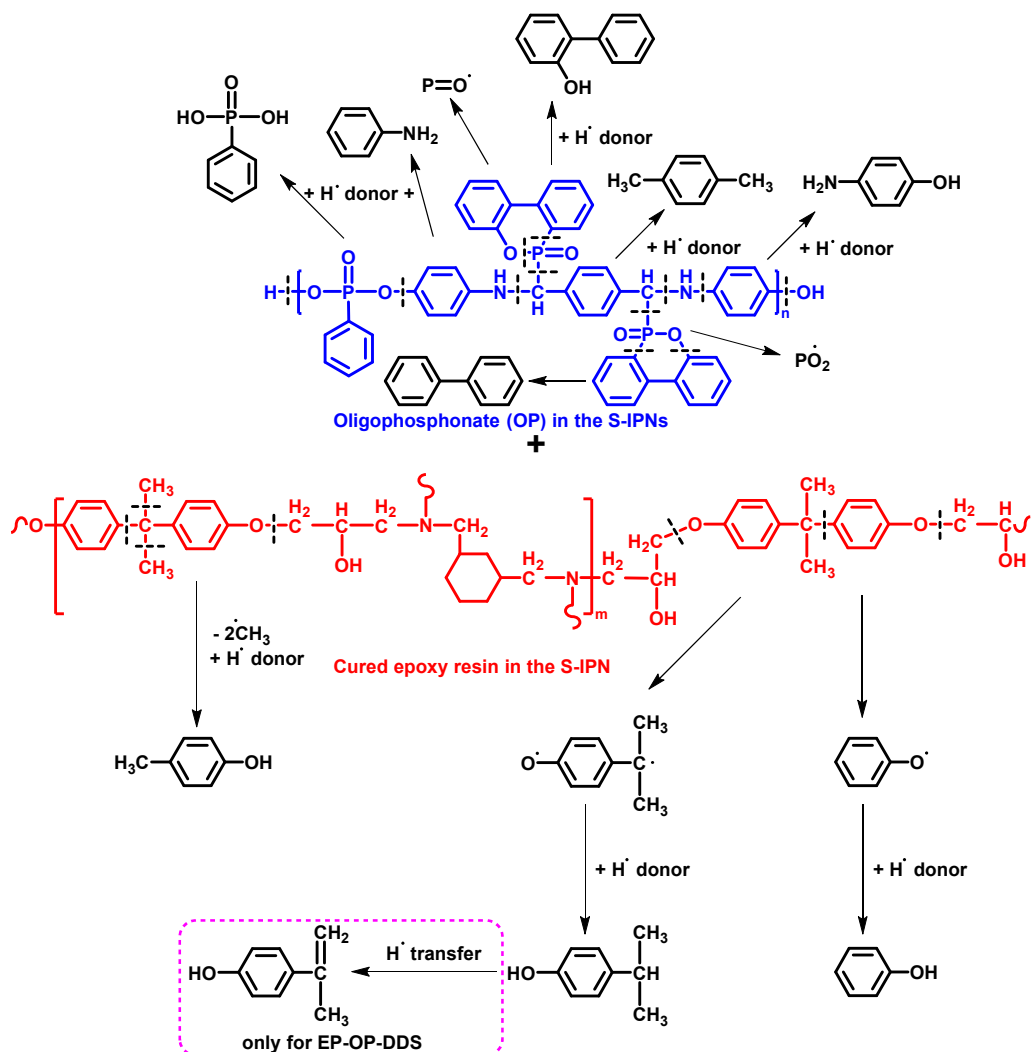
Scheme 3. Oversimplified proposed thermal decomposition mechanism of the OP/S–IPN.

Table 4 and Scheme 3 indicate entities similar to those reported in the literature. Since the degradation occurs in the presence of phosphoric derivatives, the phosphorus radicals play a crucial role in the reduction of released heat.

The presented data shows that the identified gaseous fragments may be classified into several groups: (1) low molecular weight entities (e.g. PO, CO, CO_2, H_2O – identified in the TGA–FTIR spectra); (2) cleaved fragments from main chains and subsequent rearrangements (i.e. aromatic: hydrocarbons and amines); (3) entities formed by molecular fragments reorganization at high temperatures. The composition, abundance and distribution of the pyrolyzates indicate that all samples undergo thermal degradation through initiation by random cleavages in the main chains. These scissions generate chain free radicals and carbon oxides, involving hydrogen transfer processes.

2.3.3.3. Flame resistance study by MCC and UL–94 VB small scale fire test

MCC is an important method in evaluating the combustion behavior of polymers, providing indispensable information regarding fire risks through parameters like: the heat release rate (HRR), peak of heat release rate (p–HRR), total heat release (THR) and char yield. By integrating the HRR over the entire time range (convert into temperature in Figure 11) the total heat capacity (THC) values are obtained. Table 5 shows these main combustion parameters for various formulations. From the data in Table 5 one may observe that the OP exhibited the lowest values for all parameters, while leaving the highest residue value (35.03 %). This is in a good agreement with the TGA data. The enhanced flame resistant capacity of the S–IPNs resides in lower THR values and significantly lower HRC and p–HRR values compared to OP free cured matrices. For example, p–HRR values decrease with 55.4 % (EP–OP–CYDM vs. EP–CYDM), 38.9 % (EP–OP–8CH$_2$DA vs. EP–8CH$_2$DA) and 33.08 % (EP–OP–DDS vs. EP–DDS). From a practical standpoint, such reduction in the peak heat release rate increases the time of escaping during a fire incident. The HRR curve shape of the OP showed a wide peak with a reduced shoulder at low temperature values (Figure 11). The shoulder appears due to the combustion

behavior of the OP. During combustion OP generates a thin unstable carbonaceous layer further eliminated at higher temperatures by the vigorous gases evolvement [4]. This transition disappears after introducing the OP into the S–IPNs. On close analysis of MCC data, it may be considered that the EP–OP–CYDM and EP–OP–DDS formulations have comparable parameters, the THR being much lower for the latter. EP–OP–DDS yields the highest char residue values and a superior thermal stability compared to EP–OP–CYDM, also in accordance with TGA, DSC and morphological analyses. The EP–OP–DDS is also the sole formulation to achieve a V–0 rating, while the other structures showed no classification (NC), even the two S–IPNs with the same phosphorus concentration. A content of 2 % phosphorus is not enough to achieve a V–0 rating for the S–IPNs cured with the cycloaliphatic and aliphatic hardener. This aspect may be explained by the fact that the aliphatic hardeners's polymer chains contain an increased number of methylene ($-CH_2-$) groups which decompose and release the corresponding hydrocarbon gases at specific temperatures, thus lowering their thermal stability and char yield [20]. The actual contribution of the cylcloaliphatic and aliphatic curing agents to improve the flame retardancy of the epoxy resin is limited. Based on this observation, the EP–OP–DDS S–IPN may be considered the most suitable candidate to use in various applications. The higher content of phosphorus rich char within the S–IPNs, as compared to their virgin counterparts, suggests the condensed phase flame retardant mechanism.
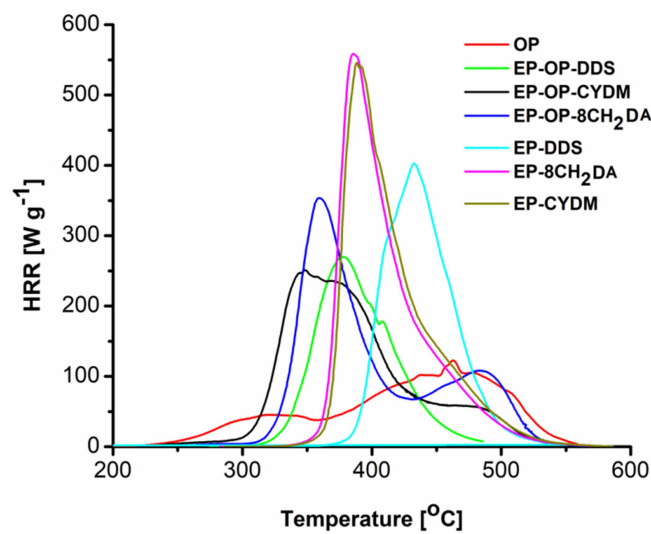
Figure 11. HRR of the OP and networks.

Table 5. UL–94 VB classification and MCC parameters of the OP and networks.

Sample	UL–94 VB	THR[a] (kJ g^{-1})	HRC[b] (J g^{-1} K^{-1})	p–HRR[c] (W g^{-1})	$W_{600\,^oC}$[d] (%)
OP	–	17.70	125.67	116	35.03
EP–OP–DDS	V–0	19.13	270.33	269	23.63
EP–OP–CYDM	NC	25.50	250.33	256	7.41
EP–OP–8CH$_2$DA	NC	26.53	347.67	352	5.56
EP–DDS	NC	24.7	411.33	402	12.02
EP–CYDM	NC	30.93	560.67	574	4.87
EP–8CH$_2$DA	NC	31.53	568.33	576	4.57

[a]Total heat release at 600 ^oC; [b]Heat release capacity; [c]Heat release rate peak; [d]Char yield at 600 ^oC

Stage 3. Accelerated UV aging correlated with flame resistance capacity of the S–IPNs
Activity 3.1. Photochemical behavior study of the S–IPNs
3.1.1. Evaluation of the influence of wavelength and irradiation intensity
The samples were exposed up to 500 h of UV irradiation with the aid of a UVP–B–100AP medium pressure mercury lamp (100 W), provided with an optical filter with maximum transparency at 365 nm, equipped with a fan. The irradiance values at 365 nm were measured with a PMA 2100 radiometer equipped with a PMA 2110 detector with spectral response between 320 and 400 nm (UVA), and the value at the sample surface was 110 W m^{-2}. The radiant exposure measured for 1 h of irradiation was 161.5 kJ m^{-2}. These values approximate 305 days of exposure to natural light

simulated into 500 h of laboratory accelerated UV exposure. The irradiation was performed in air, at 25 ± 3 °C and a relative humidity of 40%. The samples were extracted from the irradiation device at intervals of 100, 200, 300, 400 and 500 h and analyzed.

3.1.2. Investigation of surface properties by SEM–EDX

Figure 12 shows the SEM micrographs (surface and in section) of the S–IPNs before and after 500 h of UV irradiation, respectively. During the thermal treatment to obtain the S–IPNs, the OP agglomerates generated in them uniform and parallel fracture lines (Figures 12a,b). The uniform distribution of the micro fractures in the S–IPNs is an indication of the homogeneous dispersion of the OP into the cured epoxy resin. The aggressive action of the UV irradiation generates visible cracks on the surfaces of the samples and a series of irregular shapes, which seem to appear on both the surface and into the mass of the materials, underneath the physically observable cracks (Figures 12c,d). The section SEM micrographs of the S–IPNs also indicate discontinuities, and cracks into their linear and relatively uniform aspect (Figure 12d). The EP–OP–DDS S–IPN exhibits a 'sea–island' morphology type of a hand–like shape after UV irradiation (Figure 12d, on the left). The EDX profiles of the photoirradiated S–IPNs show lower carbon, nitrogen and relatively the same phosphorus contents and higher oxygen percentage, due to photo-oxidation (Figure 12(b) – right) as compared to the ones of the initial S–IPNs reported in Stage 2 of the project (Figure 3(c)). Only the EP–OP–8CH$_2$DA S–IPN shows slightly lower oxygen content after photodegradation, due to more advanced decomposition of hydroperoxide intermediates.
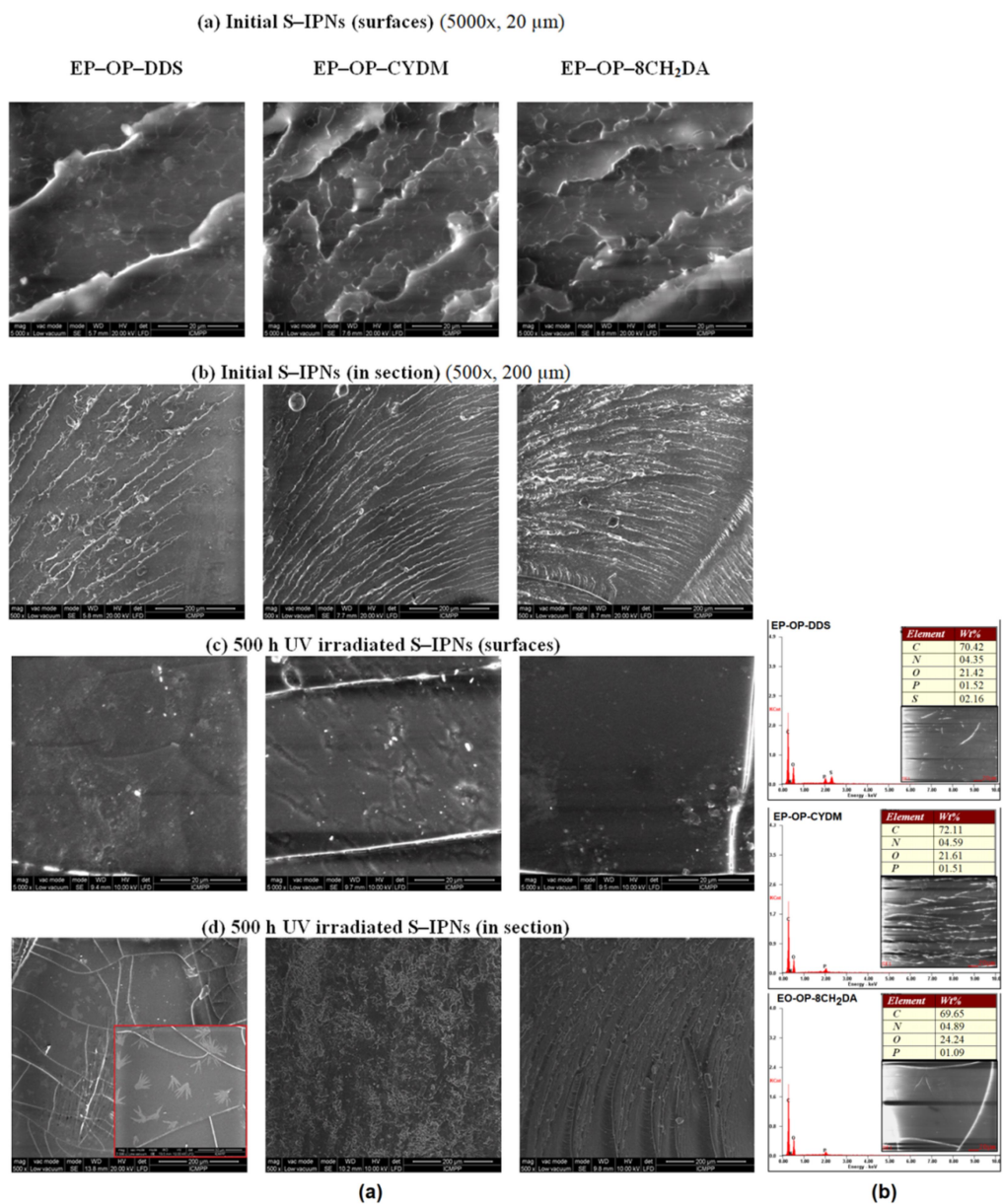
Figure 12. SEM (a) and EDX (b) images of the S–IPNs after 500 h of photoirradiation.

3.1.3. Determination of optical (color) and structural (UV-Vis) properties
3.1.3.1. Color modifications during UV irradiation
3.1.3.1.1. Lightness factor variation (L*) during UV irradiation

The lightness factor (L*) is dependent on the structure of the samples. As it can be seen from Figure 13, the highest values were registered for the EP–OP–DDS S–IPN sample recorded before exposure, for which a mean value of parameter L* = 54.3 was found. The brightness of the sample gradually decreased to 38.7 (ΔL^* = −15.6) after 500 h of UV exposure. Therefore, the negative value of ΔL^* is an indication of sample darkening during the 500 h of exposure. For the EP–OP–8CH$_2$DA sample, an initial average value of L* was found to be lower (L* = 46.7), with the surface of the material darker than EP–OP–DDS.
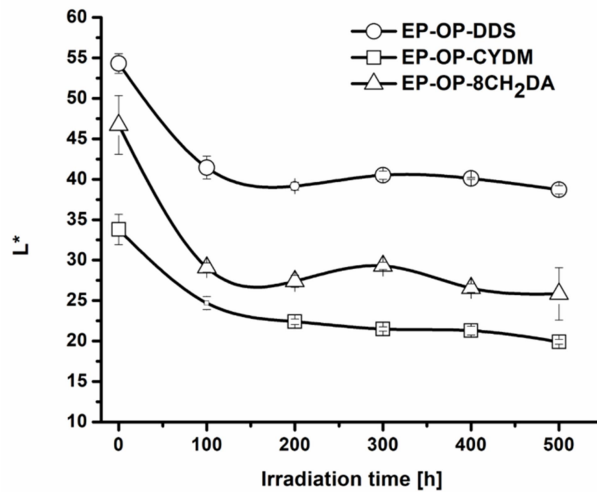
Figure 13. Variation of the L* parameter with irradiation time.

In this case, the sample is blackened during irradiation, so that after 500 h of exposure the measured value of L* is reduced to 29.1 (ΔL^* = −20.9). The more negative value of ΔL^* indicates a higher darkening tendency of S–IPN EP–OP–8CH$_2$DA compared to EP–OP–DDS. The EP–OP–CYDM S–IPN is characterized by the lowest initial L* value (L* = 33.8). However, the L* value decreased the least after 500 h of exposure, being 19.9 (ΔL^* = −13.9).

3.1.3.1.2. Variation of chromatic parameter a* during UV irradiation

The variation of the chromatic parameter a* with irradiation time is shown in Figure 14. The chromatic parameter describing the red↔green axis (a*) increases slightly with exposure time for EP–OP–DDS (Δa^* = 4.47) and EP–OP–8CH$_2$DA (Δa^* = 7.26) samples after 400 h of UV exposure, correlated with accumulation of red chromophores on the surface. However, the new colored structures are photochemically unstable, because prolonging the exposure to 500 h reduces Δa^* differences to 1.94 for EP–OP–DDS and to 5.86 for EP–OP–8CH$_2$DA. The UV irradiation decreases the red color saturation for S–IPN EP–OP–CYDM. The Δa^* values are negative during the entire exposure time, and the differences are maximal after 500 h (Δa^* = −6.92).
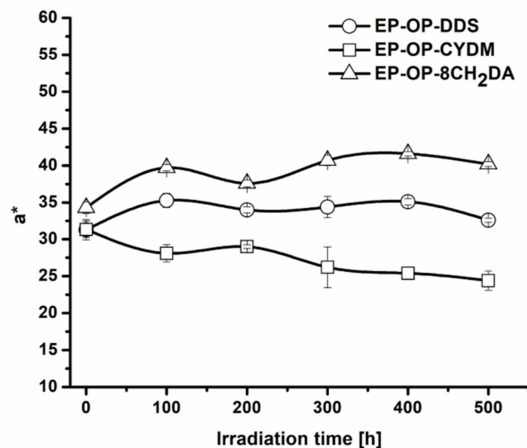
Figure 14. Variation of the a* parameter with irradiation time.

3.1.3.1.3. Variation of chromatic parameter b* during UV irradiation

The parameter b^*, representing the yellow ↔ blue color axis, shows only positive values (Figure 15). This aspect indicates the formation of yellow chromophores on the surfaces of the S–IPNs, whose concentration depends on their structure. The color saturation of the non–irradiated samples decreases in the order: EP–OP–DDS > EP–OP–8CH$_2$DA > EP–OP–CYDM. However, yellow chromophores are unstable to UV action. The b^* values decrease continuously and faster in the first 100 h of irradiation, with Δb^* values ranging between −15.0 for EP–OP–DDS and −22.6 for EP–OP–8CH$_2$DA. The S–IPN EP–OP–CYDM had and intermediate Δb^* value (−19.6) at the end of UV exposure. The Δb^* values specific to the irradiated samples were: −33.5 for EP–OP–DDS, −29.5 for EP–OP–8CH$_2$DA and −23.3 for EP–OP–CYDM.
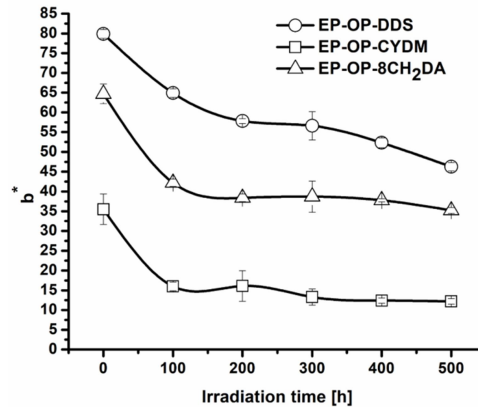
Figure 15. Variation of the b^* parameter with irradiation time.

3.1.3.1.4. Variation of ∆E values during UV irradiation

The global color modification as a result of UV exposure was calculated with equation (5) considering all the color parameters variation during irradiation, where the $\Delta E_{L*,a*,b*}$, ΔL^*, Δa^* and Δb^* are the global color modifications and the differences between the chromatic parameters of irradiated and non-irradiated samples, measured at certain time intervals.

$$\Delta E_{L*,a*,b*} = \sqrt{\Delta L *^2 + \Delta a *^2 + \Delta b *^2}$$ (5)

Figure 16 shows that ΔE_{L*a*b*} values increase in parallel with UV exposure time. It can be seen that, after 500 h of exposure, the largest global color changes were recorded in the case of the S–IPN EP–OP–8CH$_2$DA followed by EP–OP–DDS, while for the EP–OP–CYDM sample the global changes are smaller.
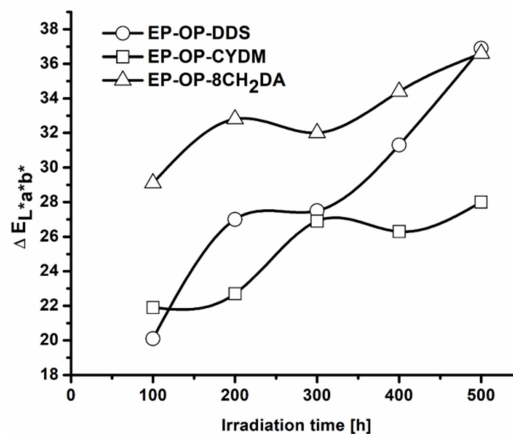
Figure 16. Color differences variation with exposure time.

3.1.3.2. Structural modifications during UV irradiation by UV–Vis

The UV–Vis reflectance spectra of the S–IPNs (Figure 17) show significant decreases in reflectance in the visible domain (400–800 nm) for all samples after 500 h of UV irradiation. The decrease of reflectance value could be correlated with a higher sensitivity of the samples to photodegradation, due to increase of light absorbance capacity.
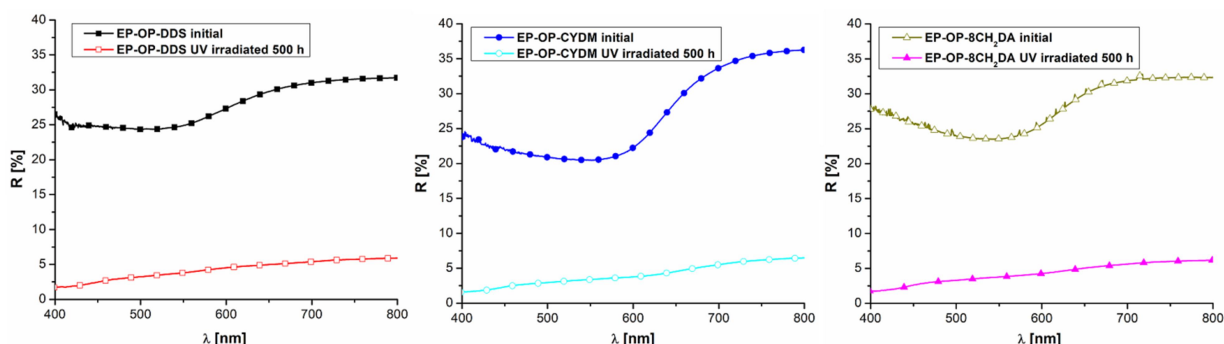
Figure 17. Reflectance spectra of the S–IPNs before and after photodegradation.

3.1.4. Correlation between photochemical behavior and flame resistance capacity of the S–IPNs

The results of the flame resistant capacity measurements of the photo-irradiated S–IPNs are summarized in Figure 18. The table from Figure 18c depicts the MCC parameters of the initial S–IPNs, reported in Stage 2 of the project, for comparison. From Figure 18c it was reported that the p–HRR values decrease with 55.4% (EP–OP–CYDM vs. EP–CYDM), 38.9% (EP–OP–8CH$_2$DA vs. EP–8CH$_2$DA) and 33.08% (EP–OP–DDS vs. EP–DDS). As one may observe from Figures 18a–c, UV irradiation leads to a decline in the fire performance of the S–IPNs. This is reflected through the seemingly increased MCC parameters of the irradiated S–IPNs compared to the ones of the initial samples, especially the HRC and p–HRR values. The HRC values of the S–IPNs increase: from 270.33 J/g K to 288.33 J/g K for EP–OP–DDS, from 250.33 J/g K to 297 J/g K for EP–OP–CYDM and from 347.67 J/g K to 425.67 J/g K for EP–OP–8CH$_2$DA. The p–HRR values of the S–IPNs also increase: from 269 W/g K to 292.1 W/g for EP–OP–DDS, from 256 W/g to 299.23 W/g for EP–OP–CYDM and from 352 W/g to 421.53 W/g for EP–OP–8CH$_2$DA. The data indicate that the exposure to UV light has a damaging effect on the S–IPNs through polymer chain scissions.
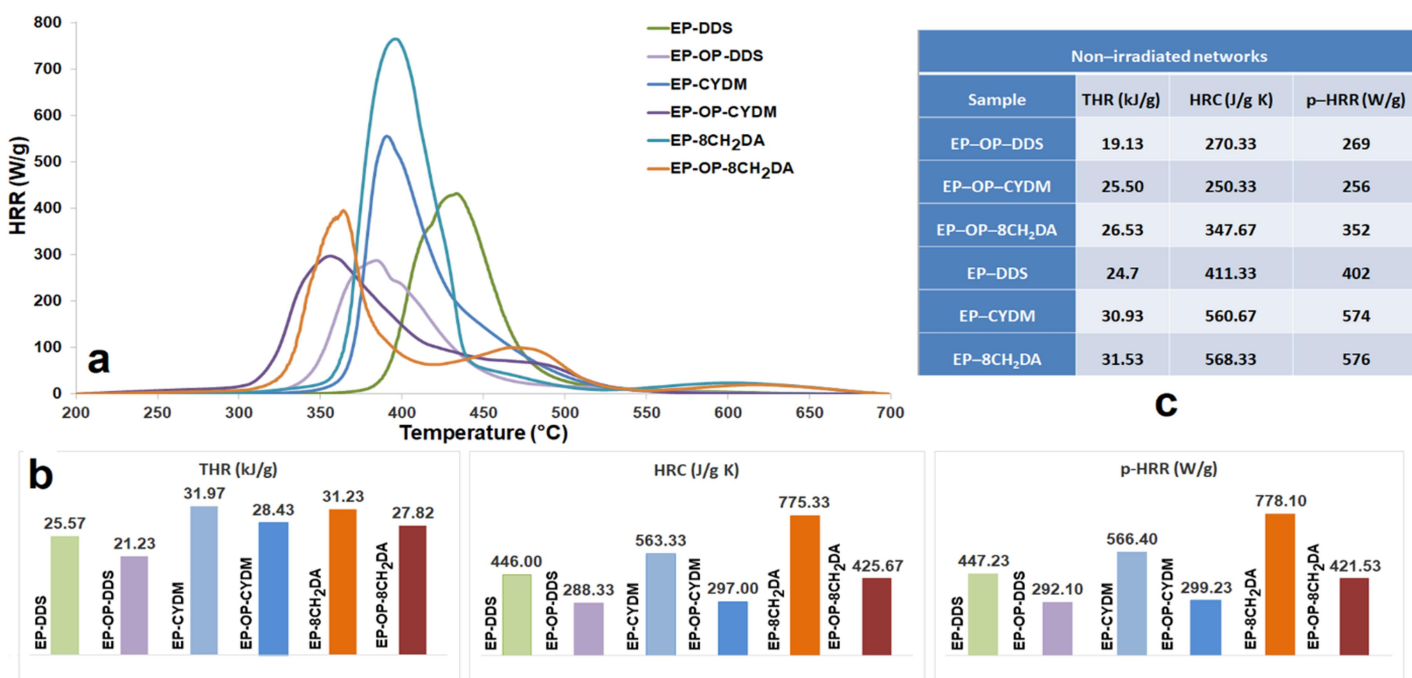
Figure 18. (a) HRR and (b) MCC data of UV irradiated samples; (c) table of MCC data of non–irradiated samples.

Activity 3.2. Promoting the project visibility

The project database has been updated and can be found at: https://icmpp.ro/epoxyphosdeg/index.php.

The involved research team in the project realized the following activities: (i) monthly work sessions with team members; (ii) counseling activities for postdoctoral students by senior researchers; (iii) organizing panels of senior scientific team problem solving; (iv) elaboration and submitting articles for publication in ISI journals; (v) establishing and procurement of the necessary materials for the development research program; (vi) human resources, financial and material planning for the next stage; (vii) acquisition activity planning, preparing documentation for procurement; (viii) tracking the supply flow and the use of funds; (ix) preparing the synthetic report for all project periods. In order to

develop and implement management structure, team members met monthly and established detailed activity plans. It was followed effective and efficient communication of administrative, technical and financial research both within the team, and with the contracting authority. The entire research team was involved in drafting the final synthetic report.

Activity 3.3. Dissemination of the results obtained throughout the entire project implementation
The obtained results during the implementation of the project where disseminated in: *7 scientific articles* published in international journals (*cumulated I.F. = 42.171*), *3 oral communications* and *10 posters* presented at national (2) and international (4) scientific conferences.

The estimated obtained impact, emphasizing the most significant results
The obtained scientific results and their impact, from the analysis of the material presented in the final report are:
- ✓ The precursor to the OP and the OP were synthesized and their structures confirmed by ^{1}H–NMR and FTIR techniques. The OP was also characterized by SEM–EDX and GPC techniques.
- ✓ Flame retardant S–IPNs were obtained based on an OP and an epoxy resin cured with three different hardeners: DDS, CYDM and 8CH$_2$DA and their structural and morphological characterization undertaken by FTIR and SEM–EDX.
- ✓ The samples resistance against decay was tested against three different wood decaying fungal strains: *Penicillium chrysogenum*, *Cladosporium cladosporioides* and *Aspergillus brasiliensis*.
- ✓ The S–IPNs exhibited very good fungistatic properties against *C. cladosporioides* and presented a general long time antifungal resistance.
- ✓ The S–IPNs DSC curves showed a good miscibility of the OP in the cured epoxy resin.
- ✓ TGA measurements were assessed in both inert and thermo–oxidative atmospheres.
- ✓ The non–isothermal kinetic parameters of the thermal degradation reactions were calculated with the isoconversional methods of Friedman and Ozawa–Flynn–Wall and indicated that the structures decompose following complex mechanisms in two or three stages depending on the chemical structure of the curing agent.
- ✓ *SEM, TGA, DSC and MCC demonstrated that S–IPNs were highly compact networks.*
- ✓ The flame retardant capacity of the structures was assessed with the UL 94–VB burning test and MCC method.
- ✓ TGA–FTIR and Py–GC–MS analyses were used to determine the evolved gaseous fragments of the samples during thermal degradation.
- ✓ A thermal degradation mechanism was proposed.
- ✓ All obtained data indicated that the EP–OP–DDS system may be considered the best candidate in different applications. For example it could be used as/or in a flame retardant coating, due to the phosphine oxide group generating miscibility and adhesion to various substrates, or as a matrix for flame retardant composites.
- ✓ The obtained data demonstrated that the flame retardant mechanism of the S–IPNs occurred in both gas and condensed phase. In the gas phase, the OP yielded phosphorus containing radicals (PO•, PO$_2$•), acting as scavengers for active H and OH based radicals from the flame area to inhibit combustion. In the condensed phase, phenyl phosphoric acid, generated in early pyrolysis stages, promotes dehydration and carbonization of the matrix and thus leading to an increasing of the residual carbon quantity. The phosphorus rich high char layer content isolated the matrix from both heat and oxygen.
- ✓ The networks exhibited color modifications and structural degradation during UV exposure. This aspect was reflected in morphological and structural modifications.
- ✓ *A significant impact of incorporating the OP into the S–IPNs resided in surface compactness during thermal degradation leading to decrease in volatiles evolvement as compared to the pristine OP.*
- ✓ *An overall significant aspect is that, although a surface phenomenon, UV irradiation contributes to decreasing the flame retardant capacity of the S–IPNs, hence affecting the bulk of the materials.*
- ✓ *In the present phase of research, the S–IPNs are not yet recommended for outdoor light exposure. It is therefore that the conducted research to this point constitutes a valuable basis towards finding suitable photostabilizers for the S–IPNs in the future.*

The originality and innovation of the objectives within the research project: **The behaviour of new multicomponent polymeric systems in simulated environmental conditions for flame retardant coating materials**, acronym: **EPOXYPHOSDEG,** for the stimulation of independent young research teams **(PN-III-P1-1.1-TE-2019-0604)**, consisted in the synthesis of new S–IPNs based on epoxy resin crosslinked with three different hardeners and OP as potential coating materials, and the correlation of their thermal degradation and accelerated UV aging with their flame resistance, as well

as their antifungal testing, a subject still not discussed or insufficiently described in the specialized literature. A new interdisciplinary approach was pursued and achieved in forming a group and future subfield in the characterization of flame retardant materials. The relevance of the project is reflected in fundamental knowledge, the educational field through the establishing of new international collaborations (**Dr. Sabyasachi Gaan -** Laboratory for Advanced Fibers, Empa, Swiss Federal Laboratories for Materials Science and Technology, St. Gallen, Switzerland (3 articles) and **Dr. Aurelio Bifulco** - School of Polytechnic and Basic Sciences, University of Naples Federico II, Department of Chemical, Materials and Production Engineering, Fuorigrotta, Naples, Italy (2 articles)) and the fields of technological and economic research by generating some guidelines towards efficient design of materials.

Final dissemination results:
Articles (7)
1. L. Rosu, F. Mustata, D. Rosu, C.–D. Varganici, I. Rosca, T. Rusu, Bio-based coatings from epoxy resins crosslinked with a rosin acid derivative for wood thermal and anti–fungal protection, ***Progress in Organic Coatings*** *151*, 106008***, 2021*** **(IF=6.206)**

2. L. Rosu, C.–D. Varganici, D. Rosu, S. Oprea, Effect of Thermal Aging on the Physico-Chemical and Optical Properties of Poly(ester urethane) Elastomers Designed for Passive Damping (Pads) of the Railway, ***Polymers*** *13(2), 192,* ***2021*** **(IF=4.967)**

3. C.–D. Varganici, L. Rosu, S. Lehner, C. Hamciuc, M. Jovic, D. Rosu, F. Mustata, S. Gaan, Semi–interpenetrating networks based on epoxy resin and oligophosphonate: Comparative effect of three hardeners on the thermal and fire properties, ***Materials & Design*** *212,* 110237***, 2021*** **(IF=9.417)**

4. F. Mustata, D. Rosu, C.–D. Varganici, L. Rosu, I. Rosca, N. Tudorachi, Assessing the thermal and fungal behavior of eco-friendly epoxy thermosets derived from vegetable oils for wood protective coatings, ***Progress in Organic Coatings*** *163,* 106612***, 2022*** **(IF=6.206)**

5. A. Bifulco, C.–D. Varganici, L. Rosu, F. Mustata, D. Rosu, S. Gaan, Recent advances in flame retardant epoxy systems containing non-reactive DOPO based phosphorus additives, ***Polymer Degradation and Stability*** *200,* 109962***, 2022*** **(IF=5.204)**

6. C.–D. Varganici , L. Rosu**,** A. Bifulco, D. Rosu, F. Mustata, S. Gaan, Recent advances in flame retardant epoxy systems from reactive DOPO–based phosphorus additives, ***Polymer Degradation and Stability*** *202,* 110020, ***2022*** **(IF=5.204)**

7. C.–D. Varganici, L. Rosu, D. Rosu, C. Hamciuc, I. Rosca, A.–L. Vasiliu, Effect of hardener type on the photochemical and antifungal performance of epoxy and oligophosphonate S–IPNs, ***Polymers*** *14(18),* 3784***, 2022*** **(IF=4.967)**

Oral communications (3)
1. C.–D. Varganici, L. Rosu, D. Rosu, F. Mustata, Epoxy–based S–IPNs as eco–friendly flame retardants, ***6th Central and Eastern European Conference on Thermal Analysis and Calorimetry and 15th Mediterranean Conference on Calorimetry and Thermal Analysis (CEEC-TAC6 & Medicta2021), Split, Croatia, July 20-24, 2021***.

2. I. Rosca, C.–D. Varganici, L. Rosu, C. Hamciuc, D. Rosu, F. Mustata, Antifungal properties of new multicomponent polymer systems as flame retardant coatings, ***Progress in Organic and Macromolecular Compounds Conference - MACRO Iasi, Romania, October 7-9, 2021***.

3. M.–F. Zaltariov, C.–D. Varganici, D. Filip, D. Macocinschi, Stability of the HPC/PU polymeric blends in accelerated weathering and biological environments, ***1st Corrosion and Materials Degradation WEB Conference (On-line), May 17-19, 2021***.

Posters (10)
1. C.–D. Varganici, L. Rosu, F. Mustata, D. Rosu, I. Rosca, Thermal behaviour and fungal protection of composites based on wood and natural and synthetic epoxy resins cured with a rosin acid derivative, ***6th Central and Eastern European Conference on Thermal Analysis and Calorimetry and 15th Mediterranean Conference on Calorimetry and Thermal Analysis (CEEC-TAC6 & Medicta2021), Split, Croatia, July 20-24, 2021***.

2. L. Rosu, C.–D. Varganici, F. Mustata, D. Rosu, Thermal characterization of bio–based epoxy resins crosslinked with curing agents from raw renewable resources, ***6th Central and Eastern European Conference on Thermal Analysis and Calorimetry and 15th Mediterranean Conference on Calorimetry and Thermal Analysis (CEEC-TAC6 & Medicta2021), Split, Croatia, July 20-24, 2021***.

3. L. Rosu, C.–D. Varganici, F. Mustata, D. Rosu, A.–L. Vasiliu, Non-isothermal degradation kinetic study of new multicomponent polymer systems for flame retardant coatings, ***6th Central and Eastern European Conference on***

Thermal Analysis and Calorimetry and 15ᵗʰ Mediterranean Conference on Calorimetry and Thermal Analysis (CEEC-TAC6 & Medicta2021), Split, Croatia, July 20-24, 2021.

4. A.–L. Vasiliu, C.–D. Varganici, D. Rosu, F. Mustata, O.–M. Munteanu, L. Rosu, Morphological study of some epoxy resin with DOPO–based oligophosphonate S-IPNs, *Progress in Organic and Macromolecular Compounds Conference - MACRO Iasi, Romania, October 7-9, 2021*.

5. L. Rosu, A.–L. Vasiliu, C.–D. Varganici, D. Rosu, F. Mustata, Epoxy and oligophosphonate S–IPNs. Morphological study, *Polymers 2022 - New Trends in Polymers Science: Health of the Planet, Health of the People, Turin, Italy, May 25-27, 2022.*

6. C.–D. Varganici, L. Rosu, D. Rosu, Effect of UV irradiation on epoxy and oligophosphonate S–IPNs, *Polymers 2022 - New Trends in Polymers Science: Health of the Planet, Health of the People, Turin, Italy, May 25-27, 2022.*

7. L. Rosu, C.–D. Varganici, D. Rosu, Thermal degradation study of S–IPNs based on epoxy resin and oligophosphonate, *22ⁿᵈ Romanian International Conference on Chemistry and Chemical Engineering (RICCCE 22), Sinaia, Romania, September 7-9, 2022.*

8. C.–D. Varganici, L. Rosu, D. Rosu, Photochemical behaviour of flame retardant epoxy and oligophosphonate systems, *22ⁿᵈ Romanian International Conference on Chemistry and Chemical Engineering (RICCCE 22), Sinaia, Romania, September 7-9, 2022.*

9. L. Rosu, C.–D. Varganici, D. Rosu, F. Mustata, Study on the non-isothermal decomposition kinetics of new S-IPNs designed as flame retardants, *XXXVIᵗʰ National Chemistry Conference, Calimanesti-Caciulata, Romania, October 4-7, 2022.*

10. C.–D. Varganici, D. Rosu, F. Mustata, L. Rosu, Thermal behavior study of some bio-based epoxy resins, *XXXVIᵗʰ National Chemistry Conference, Calimanesti-Caciulata, Romania, October 4-7, 2022.*

The project database has been updated and can be seen at: https://www.icmpp.ro/epoxyphosdeg/.
The research team has met its objectives with a total degree of achievement.

Project Manager,
Dr. Cristian-Dragos Varganici
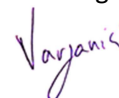
References
[1] R.M. Silverstein, F.S. Webster, D.J. Kiemle, *Spectrometric Identification of Organic Compounds*, Seventh ed., John Wiley & Sons, **2005**; [2] G. Socrates, *Infrared and Raman Characteristic Group Frequencies: Tables and Charts*, Third ed., Wiley, Chichester, **2004**, p. 366; [3] D. Rosu, L. Rosu, F. Mustata, C.D. Varganici, *Polym. Degrad. Stab.* 97 (**2012**) 1261–1269; [4] I.–D. Carja, D. Serbezeanu, T. Vlad–Bubulac, C. Hamciuc, A. Coroaba, G. Lisa, C.G. López, M.F. Soriano, V.F. Pérez, M.D.R. Sánchez, *J. Mater. Chem. A* 2 (**2014**) 16230–16241; [5] C.–D. Varganici, L. Rosu, D. Rosu, B.C. Simionescu, *Compos. Part B: Eng.* 50 (**2013**) 273–278; [6] D. Rosu, L. Rosu, C.–D. Varganici, *J. Anal. Appl. Pyrolysis* 100 (**2013**) 103–110; [7] I. Butnaru, C.–D. Varganici, M. Pinteala, S. Lehner, M. Bruma, S. Gaan, *J. Anal. Appl. Pyrolysis* 134 (**2018**) 254–264; [8] S. Vyazovkin, A.K. Burnham, J.M. Criado, L.A. Pérez–Maqueda, C. Popescu, N. Sbirrazzouli, *Thermochim. Acta* 5 (**2011**) 1–19; [9] D. Rosu, C.N. Cascavaf, C. Ciobanu, L. Rosu, *J. Anal. Appl. Pyrolysis* 72 (2004) 191–196; [10] C.–D. Varganici, D. Rosu, C. Barbu–Mic, L. Rosu, D. Popovici, C. Hulubei, B.C. Simionescu, *J. Anal. Appl. Pyrolysis* 113 (**2015**) 390–401; [11] M. Worzakowska, Polymer 48 (**2007**) 1148–1154; [12] M. Edelmann, M. Gedan–Smolka, G. Heinrich, D. Lehmann, *Thermochim. Acta* 452 (**2007**) 59–64; [13] J. Opfermann, *J. Therm. Anal. Calorim.* 60 (**2000**) 641–658; [14] L. Jiang, P. Zhang, L. Dong, K. Liu, *J. Therm. Anal. Calorim.* 138 (**2019**) 3031–3037; [15] D. Rosu, L. Rosu, M. Brebu, *J. Anal. Appl. Pyrolysis* 92 (**2011**) 10–18; [16] L.D. Field, H.L. Li, A.M. Magill, *Organic Structures from Spectra*, Sixth ed., John Wiley & Sons, Hoboken, **2020**; [17] W. Xie, W.–P. Pan, K.C. Chuang, *J. Therm. Anal. Calorim.* 64 (**2001**) 477–485; [18] A. Bifulco, D. Parida, K.A. Salmeia, S. Lehner, R. Stämpfli, H. Markus, G. Malucelli, F. Branda, S. Gaan, *Compos. Part C: Open Access* 2 (**2020**) 100022; [19] A. Bifulco, D. Parida, K.A. Salmeia, R. Nazir, S. Lehner, R. Stämpfli, H. Markus, G. Malucelli, F. Branda, S. Gaan, *Mater. Design* 193 (**2020**) 108862; [20] P. Deng, Y. Liu, Y. Liu, C. Xu, Q. Wang, *Polym. Adv. Technol.* 29 (**2018**) 1294–1302.